

ABSTRACT

Title of Thesis: **ROBUST CONTROL OF AN EVTOL
THROUGH TRANSITION WITH
A GAIN SCHEDULING LQR CONTROLLER**

Derek Thompson
Master's of Science, 2020

Thesis Directed by: Huan Xu
Department of
Aerospace Engineering

The advancements in electric motor propulsion and battery technologies have made the implementation of electric power in aerial transportation increasingly feasible. As such, the interest and development of electric vertical takeoff and landing (eVTOL) aircraft has become a greater portion of the market. This increase drives a need for research into control of the eVTOLs to ensure safe flight through the transition from hover to forward flight. This paper proposes a control strategy using the transition dynamics in a gain scheduling LQR attitude controller to robustly control the vehicle at any point throughout transition. The proposed control strategy is tested through implementation in nonlinear 3DOF and 6DOF simulations. The robustness of the controller is tested through simulating transition and virtual mission profiles.

ROBUST CONTROL OF AN EVTOL THROUGH TRANSITION
WITH A GAIN SCHEDULING LQR CONTROLLER

by

Derek Thompson

Thesis submitted to the Faculty of the Graduate School of the
University of Maryland, College Park in partial fulfillment
of the requirements for the degree of
Master's of Science
2020

Advisory Committee:
Professor Huan Xu, Chair/Advisor
Professor Derek A. Paley
Professor Micheal Otte

© Copyright by
Derek Thompson
2020

Acknowledgments

I would like to thank everyone who has helped me throughout my career as a student at the University of Maryland and everyone who has helped me get to where I am now. I need to first extend my greatest thanks to my advisor, Mumu Xu. I have worked on many exciting projects and have learned so much from everything I have done. I consider myself lucky to have had the opportunities to experience working on these problems with such an exceptional set of people.

Next, I have to thank everyone I have worked with on projects and everyone who is or has been apart of XLab while I have been here. I have met so many people that have helped me and taught me lessons I will never forget. Working with such a diverse set of individuals has been more helpful to me then any project I have been a part of. I hope I was able to give to those around me as much as I know they helped me.

I would like to thank the University of Maryland Aerospace Department and all the professors I have had during my tenure here. It was not always easy, but I feel I am prepared to face whatever comes next. Additionally, I am thankful for all the other worker that make up the backbone of this institution. Without them the opportunities I have been given would not exist.

The Hop Flyt team down in southern Maryland has been the reason for my involvement in this project and I need to thank them for it. I specifically need to thank Rob Winston, Rory Feely, and Scott Zupancic. The team has high ambitions and I know they can get it done. Best of luck to everyone down there and I am

looking forward to the first flight test.

Finally, I want to thank my family and friends for keeping me sane during the last six years. Here's to whatever is next.

Table of Contents

Acknowledgements	ii
Table of Contents	iv
List of Tables	v
List of Figures	vi
List of Abbreviations	viii
1 Introduction	1
1.1 Introduction	1
1.2 Literature Review	4
1.3 Thesis Overview	7
2 Vehicle Dynamic Model	9
2.1 Vehicle Model	9
2.2 Actuator Modeling	12
3 Control Strategy	22
3.1 Transition solver	22
3.2 Controller Design	27
4 Simulations	35
4.1 3DOF Simulation	35
4.2 6DOF Simulation	41
5 Conclusion	56
5.1 Summary of Contributions	56
5.2 Future Work	57
Bibliography	62

List of Tables

2.1	Model Properties	12
2.2	Hitec D777MG servo specifications	13

List of Figures

1.1	Venturi Vehicle	3
2.1	Vehicle Model Rendering	11
2.2	Experimental Wing Response	14
2.3	Simulated Wing Response	15
2.4	Motor Response	16
2.5	Propeller Thrust Data	18
2.6	Propeller Moment Data	19
2.7	Wing Coefficients	20
3.1	Transition Thrust Required	25
3.2	Transition Throttle Required	25
3.3	Transition Efficiency	26
3.4	Model Axis Definition	28
3.5	Model Actuator Definition	29
3.6	LQR Controller Parameter Weighting	31
3.7	LQR Controller Feedback Gain Scheduling	32
3.8	LQR Controller Pole Locations	32
3.9	Controller Overview	34
4.1	Transition Corridor Simulation	37
4.2	3DOF Transition Simulation Wing Incident angle	38
4.3	3DOF Transition Simulation Motor Output	39
4.4	3DOF Transition Simulation Attitude	40
4.5	3DOF Transition Simulation Velocity	40
4.6	3DOF Mission Simulation Wing Incident	42
4.7	3DOF Mission Simulation Motor Output	42
4.8	3DOF Mission Simulation Position	43
4.9	3DOF Mission Simulation Velocity	43
4.10	3DOF Mission Simulation Attitude	44
4.11	3DOF Mission Simulation Transition Corridor	44
4.12	6DOF Transition Simulation Wing Incident	46
4.13	6DOF Transition Simulation Motor Output	46

4.14	6DOF Transition Simulation Position	47
4.15	6DOF Transition Simulation Velocity	48
4.16	6DOF Transition Simulation Attitude	49
4.17	6DOF Mission Simulation Wing Incident	50
4.18	6DOF Mission Simulation Motor Output	51
4.19	6DOF Mission Simulation Position	52
4.20	6DOF Mission Simulation Velocity	53
4.21	6DOF Mission Simulation Attitude	54
4.22	6DOF Mission Simulation Transition Corridor	55

List of Abbreviations

eVTOL	Electric Vertical Takeoff and Landing
VTOL	Vertical Takeoff and Landing
LQR	Linear Quadratic Regulator
VTOL	Vertical Takeoff and Landing
LPV	Linear Parameter Varying
PID	Proportional Integral Derivative
RC	Radio Control
BLDC	Brushless Direct Current
3DOF	3 Degrees Of Freedom
6DOF	6 Degrees Of Freedom
LQG	Linear Quadratic Regulator
MIPS	Maryland's Maryland Industrial Partnership
Q	State Weight Matrix
R	Input Weight Matrix
γ	Wing Incident Angle
V_a	Actuator velocity
F_a	Force output from an actuator set
M_a	Moment output from an actuator set
ω_b	Body rotation rate
X_a	Actuator body position
V_b	Body velocity
l_x	Actuator X offset
l_y	Actuator Y offset
m	Vehicle mass
I	Inertia Matrix
$I_{wing,y}$	Wing actuator Y mass moment of inertia
b	Individual wing actuator span
c	Individual wing actuator chord
$l_{body,x}$	X Body length
$l_{body,y}$	Y Body length
$l_{body,z}$	Z Body length
$A_{body,x}$	YZ plane body area
$A_{body,y}$	XZ plane body area
$A_{body,z}$	XY plane body area
V_{cell}	Nominal Battery Cell Voltage
N_{cell}	Number of battery cells
KV_{motor}	Motor KV specification
ω_m	Maximum motor rotation rate

ρ	Air density
q	Dynamic pressure
Drag	Vehicle drag force
Drag _{ω}	Vehicle drag moment
C_l	Lift Coefficient
C_d	Drag Coefficient
C_m	Moment Coefficient
η	Motor power efficiency
ϕ	Roll
θ	Pitch
ψ	Yaw
ω_ϕ	Roll Rotation Rate
ω_θ	Pitch Rotation Rate
ω_ψ	Yaw Rotation Rate
X	X global position
Y	Y global position
Z	Z global position
u	State input
K	Feedback gain matrix
x	State vector
J	LQR cost parameter

Chapter 1: Introduction

1.1 Introduction

Flying cars and personal air transportation have been an icon of the future and a dream for many throughout time. Flying has mainly always been associated with large Airline companies with rigid constraints and relatively little flexibility with regards to individual travelers, however with the betterment of technology this concept is being challenged. With the improvement in electrical power systems, the interest in eVTOL (electric Vertical Takeoff and Landing) aircraft has greatly expanded [1]. The improvements in storage and the efficiency of which the energy is used have made the idea of fully electric aircraft plausible. Aircraft can adopt battery powered engines and move away from conventional fuel burning powerplants. Electric powerplants have many advantages over traditional powerplants including reduced noise, reduced environmental impact, and greater flexibility in operations [2] [3]. While the main market for eVTOLs are their potential for transport of personnel between local regions, they have applications for various other uses including medical transportation, transportation of goods, military applications, and tourism [4] [5]. Many companies see the potential in electric vehicles, in particular eVTOLs, including big name companies like Airbus, Boeing, and Uber which are starting to

develop their own eVTOL designs [6] [7] [8]. While the goal of each company is to implement a vehicle capable of commuting applications as soon as possible, the extent of the progress so far has been the creation of test vehicles and technology demonstrators. Most experts agree that the battery technology in its current state is insufficient for the deployment of full eVTOLs, but with the rapid pace of development towards the necessary technology it is important to develop the designs and operations now [9].

One of the companies striving for space in the rising eVTOL market share is the company Hop Flyt. Hop Flyt is developing their Venturi eVTOL aircraft model to provide metro region commuter services [10]. Working with the University of Maryland's Maryland Industrial Partnership(MIPS) program, this vehicle is the impetus of this research. In conjunction with the University of Maryland, Hop Flyt aimed to create a control strategy that could fully control the vehicle from hover into forward flight. The Venturi model uses four variable incident wings that can rotate to switch between forward flight and hover. On each wing the vehicle utilizes four motors and four propellers to create two sets of contra-rotating propellers. Each motor set is built into a channel structure in the wing to increase propulsive efficiency. The aircraft is controlled through the actuation of the wing incident angle and the output of the motor. During hover the vehicle full relies on the thrust from the motors produce lift. When the vehicle is in hover and in a state where it is safe to transition into forward flight, the wings simultaneously pitch forward until the vehicle gains forward velocity and can use the wings to generate significant lift. In forward flight the vehicle relies on the lift from the wing and can reduce energy

used by the motors. The vehicle is shown in fig 1.1. The objective of this research is to develop the model of the Venturi vehicle and create a robust controller to stabilize the vehicle through transition. To do this a model of the vehicle needs to be established to create a baseline for the research into the dynamics. From this the transition can be defined and a trajectory from hover to forward flight defined. With an understanding of the dynamics a robust control strategy that accounts for the changing dynamics can be developed. Finally the robustness of the controller needs to be verified through a simulation of the developed model.



Figure 1.1: Rendering of Venturi Vehicle.source:<http://hopflyt.com/venturiold/>

1.2 Literature Review

In order to develop a strategy to control the vehicle throughout transition it is important to understand current eVTOL designs and the control strategies that help them transition between flight regimes. The design of eVTOLs are classified by the method the control is transitioned into between hover and forward flight. The most common classifications of eVTOLs are Tilt-rotors, tilt-wing, Dual systems, and tail sitters [11]. Tilt-rotors employ normal aerodynamic profiles but have the ability to rotate the motors to provide vertical lift and forward thrust. As they transition into forward flight the lift generated from the wing profiles produces more lift and the motors are shifted to provide forward thrust rather than lift. Tilt-rotors are beneficial as they allow for conventional aerodynamics lift designs and only rotate the motors simplifying the design. Notable examples of this configuration includes Joby Aviation [12], the Kitty Hawk Heaviside [13] Lilium Jet [14], and Uber Elevate [7]. Closely related to tilt-rotors, tilt-wings also use rotation of the motors to provide vertical and horizontal thrust, but the motor is incorporated into the wing so the entire wing-motor system is rotated. This design allows for greater flexibility in how the motor interacts with the wing, offering greater efficiency [11]. Tilt-wing designs are employed in the Airbus Vahana [6], ASX MOBi-ONE [15], and Hop Flyt Venturi [10]. Dual system eVTOLs separate the used control actuators for each flight regime. There are a separate set of motors used for lift during hover and thrust during forward flight. This configuration allows for the simplest design but includes redundant systems leading to inefficiencies. This design is currently used

on Boeing’s PAV technology demonstrator [8]. The final configuration for eVTOLs are tail sitters. Instead of rotating the motors, the entire vehicle is rotated to use the same motors in the same configuration for hover and forward flight. This design is not seen on eVTOL designs for commuter and regional transport due to discomfort to the passenger.

During transition, the dynamics of the aircraft change significantly and characterizing them results in a highly nonlinear model. To control the vehicle there are number of methods available. One of the most common techniques to handles changing nonlinear models is employing gain scheduling [16]. Gain scheduling discretizes nonlinear dynamics into a set of linear models. The nonlinear model is converted to a Linear Parameter Varying (LPV) model, where the current model is defined by the scheduling parameter. The transition can be segmented into models based on a parameter describing the degree of transition. With each linear model a corresponding linear controller can be applied to stabilize the vehicle. Gain scheduling has been researched and tested in [17] [18] [19]. For VTOL applications the scheduling parameter also defines the transition corridor [20]. The transition corridor represents the state path the a VTOL aircraft follows during transition. This is used in conjunction with gain scheduling to create a control policy throughout transition in [21] [22]. Another method to control a vehicle through transition is a sliding mode controller. This applies a discontinuous switching control signal based on the system’s states. The switching control policies are meant to drive the system along a desired sliding surface to the desired state. This control strategy has been research in [23] [24] [25] [26]. Similarly to the sliding mode controller, the use of

fuzzy logic controllers in [27] [28] are used for VTOL applications to vary between discrete controller of different flight regimes. This approach defines the transition into fixed regimes with respective controllers and mixes the output to achieve a desired control strategy. If the dynamics of the system are well known a Nonlinear Dynamics Inversion can be used to create a control loop from complex nonlinear dynamics [11]. Using the nonlinear dynamics, a control policy can be defined that calculates the nonlinear input for a desired linear state change. This technique is used in [29] [30]. One of the most widely used controllers are Proportional Integral Derivative (PID) controller as seen in [31] [32]. By applying the state errors to a PID controller, a robust and stable output can be easily be achieved in a number of applications. Often used in conjunction with PID controllers, backstepping controllers use a nested set of control loops to achieve the desired control. Backstepping controllers can relate states through associated control loops and are researched in [33] [34]. Linear Quadratic Regulator (LQR) controllers provide optimal cost linear feedback control through the solution to the Riccati equation. Given weighting matrices Q and R relating the cost of the states and inputs respectively, the optimal linear feedback matrix can be computed as used in [35] [36] [37]. This method provides a direct way to connect the desired output to complex systems inputs like dynamics actuators in many VTOL designs which makes them very useful for VTOL applications. The control techniques presented will most often be used in conjunction with other techniques. Different control strategies can be layered to achieve mixed control loops with various methods to handle the transition nonlinearities. These procedures offer numerous methods to handle nonlinear systems and apply various

control techniques, but do not provide a succinct method to define the transition for an eVTOL and a coinciding robust controller defined by the transition.

1.3 Thesis Overview

The goal of this research is to provide a robust control strategy for the Hop Flyt Venturi vehicle. The application of eVTOL vehicles drives a need to understand the dynamics of the transition. This research will provide a method to characterize the transition and define a controller that can ensure stability at all times based on the dynamics of the vehicle. Chapter 1 presented the goal of the research and outlined the process that will be taken to get there. After this the current state of eVTOLs was discussed and the common techniques used to implement control of these aircraft were reviewed.

In chapter 2 a model of the vehicle will be developed which will be the foundation of the research and results. The vehicle will be into subsystems and each subsystem will be modeled to create an accurate representation of the full dynamics of the vehicle. This model will provide the basis for the calculations and the simulation results.

With a complete model of the vehicle, Chapter 3 will present a control strategy to control the vehicle through transition. A model of the transition will be developed which will enable the controller for use through transition. A control policy derived from the linearized vehicle dynamics will be proposed.

Chapter 4 will cover testing the robustness of the proposed control strategy. A

simulation of the full vehicle dynamics, at first modeling the longitudinal dynamics and then moving to the full dynamics of the system, will be created and the proposed control strategy from the transition linearized model is implemented. The results from the simulation give a indication of the effectiveness of the proposed strategy.

Finally, chapter 5 will discuss the result and implications of the research. It will also analyze the limitations of this research and the next steps to take.

Chapter 2: Vehicle Dynamic Model

2.1 Vehicle Model

The intent of this research is to create a method to control the vehicle into forward flight and simulate the effectiveness of this method. To do this, the dynamics needed to be simplified to create a usable model. The simplified vehicle eliminates many of the difficult to model interactions between subsystems, such as the channel propulsion interactions, variable incident wings lift profile and delayed stall from motor airfoil interactions. This is done in order to create a model that can be accurately modeled while maintaining the capability to model the transition. The final model replaces the channel propulsion systems with point forces and moments interacting at the motor mounting point on the vehicle. The motor mounting point is also modeled as the center of each wing at the quarter chord point. Each wing and motor combination is replaced with a decoupled single continuous wing and single motor. The incident angle for each actuator pair is the equivalent, modeled as angle γ about the Y axis with full forward as $\gamma = 0$. The force F_a and moment M_a of each actuator input is applied to the vehicle through the defined actuator point through [2.1](#). The total force F_{total} and moment M_{total} on the vehicle body is a sum of the effect of the body drag, F_{drag} and M_{drag} , external disturbances, F_{dist} and M_{dist} , and

the effects of the actuators. The velocity of the actuator, V_a , which influences the output of the subsystem is calculated as the local velocity of the actuator from the body velocity, V_b , and the body rotation rates, ω_b , and the position of the actuator with regards to the center of mass, X_a , in 2.2.

$$F_{total} = F_{drag} + F_{dist} + \sum F_a \quad (2.1)$$

$$M_{total} = M_{drag} + M_{dist} + \sum M_a + \sum F_a \times X_a$$

$$V_a = V_b + \omega_b \times X_a \quad (2.2)$$

The objective of this thesis is to research a control strategy for the Venturi vehicle. The proposed strategy would need to be verified on a test platform before any full scale test is attempted. Hop Flyt developed a 1/7th scale Venturi model for control testing and verification. This research contributes to testing on this platform so the vehicle properties and actuator modeling are representative of the systems on this platform. The simplified model assumes the mass and sizing properties of Hop Flyt's test vehicle. The modeled vehicle, shown in figure 2.1, is symmetric among the X and Y planes about the vehicle's center of mass. The actuator points are offset longitudinally from the center of mass a distance l_x and a lateral distance l_y .

In order to get an estimate of the Inertia matrix, the vehicle was broken down into subsystems by mass and each subsystem was estimated to build a total estimate of inertia. The model is simplified to have a fixed inertia matrix. During transition the inertia of the vehicle would vary. For simplicity during simulation, this is reduced to the average inertia in the model between hover and forward flight.

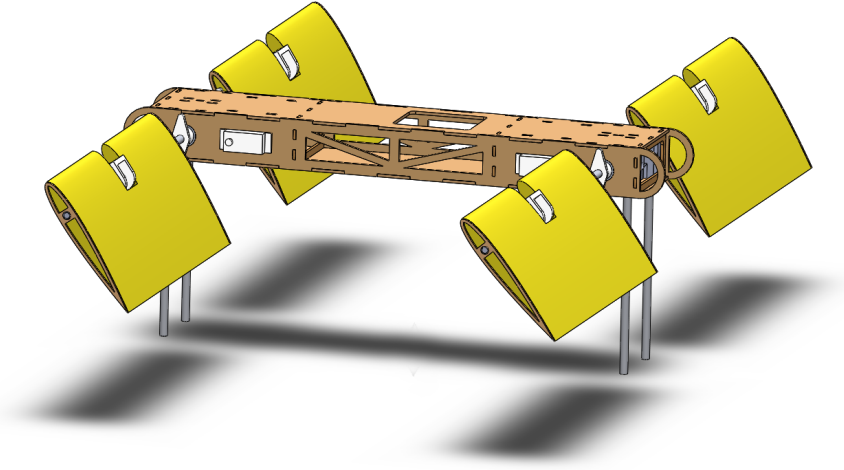


Figure 2.1: Rendering of Modeled Vehicle

If the model simulated the dynamic inertia matrix, the change in dynamics could be easily accounted for the state space design in section 3.2. The final specifications for the modeled vehicle are presented in 2.1.

The vehicle's drag is modeled as the drag from the vehicle body in addition to the drag produced from the actuators. The body drag is modeled as the dynamic pressure of the airflow on the vehicle body in 2.3. The rotational drag is calculated from integrating the velocity of the area of the body on each plane to get the average velocity of the body plane around the center of mass. Then using the rotation to approximate drag on an equivalent body area using a drag coefficient of one. This is calculated in 2.4 for the drag roll.

$$Drag = 1/2\rho\tilde{v}^2 \cdot \tilde{a}_{body} \quad (2.3)$$

m	4.2 [kg]									
I	<table border="1" style="display: inline-table; vertical-align: middle;"> <tr> <td>0.1690</td> <td>0</td> <td>-0.0156</td> </tr> <tr> <td>0</td> <td>0.1885</td> <td>0</td> </tr> <tr> <td>-0.0156</td> <td>0</td> <td>0.3251</td> </tr> </table> [kg*m ²]	0.1690	0	-0.0156	0	0.1885	0	-0.0156	0	0.3251
0.1690	0	-0.0156								
0	0.1885	0								
-0.0156	0	0.3251								
$I_{wing,y}$	0.0007464 [kg*m ²]									
l_x	0.2667 [m]									
l_x	0.2286 [m]									
b	0.4572 [m]									
c	0.1905 [m]									
$l_{body,x}$	0.127 [m]									
$l_{body,y}$	0.0762 [m]									
$l_{body,z}$	0.762 [m]									
$A_{body,X}$	0.009677 [m ²]									
$A_{body,Y}$	0.05806 [m ²]									
$A_{body,Z}$	0.09677 [m ²]									
V_{cell}	3.8 [V]									
N_{cell}	6									
KV_{motor}	920 [Hz/V]									
ω_m	21966 [rad/s*V]									

Table 2.1: Model Properties

$$Drag_\omega = \rho\omega_\phi^2(1/3)((l_{body,y}/2)^3a_{body,z} + (l_{body,z}/2)^3a_{body,y}) \quad (2.4)$$

2.2 Actuator Modeling

The aircraft model uses the characteristics of the individual actuator components to model the response of the vehicle actuators. These actuators represent off the shelf Radio Control (RC) components, namely Brushless Direct Current (BLDC) motors and servo actuators. The vehicle's two actuator controls, the wing incident angle and motor speed, are modeled as a response to the desired output in order to reproduce the physical output of the individual components. Each component

is modeled through a non-linear second order transfer functions with tabular data from the components to model the output to the system. The actuators are modeled with this for computation efficiency and simplification of the subsystem. The wing incident angle response is defined through the properties of the chosen servo, the D777MG [38]. The pitch response is sensitive to small inputs and requires rapid response particularly when in transitioned into forward flight. This servo was chosen due to its large stall torque and fast response time. The properties of the servo actuator are shown in table 2.2.

No Load speed	0.08s/60°
Stall Torque	6.48 kg-cm
Max Travel	144°

Table 2.2: Hitec D777MG servo specifications

Using the parameters of the servo, the response was modeled as a critically damped nonlinear second order transfer function with a maximum actuation speed of the servo speed and a selected natural frequency. The natural frequency was set high enough so that the response is restricted by the maximum servo speed. This method was tested with another servo, HS-55 [39]. A video of the servo response was analyzed to get the response for which the results are shown in figure 2.2.

To account for the reduction in motor response speed when the servo is under load, the modeled servo response time is doubled to represent a worst case scenario. Figure 2.3 shows the step response of the simulated wing compared to the reduced maximum speed of the actuator. The figure shows the response to 90 degrees of desired change and demonstrates that the simulated nonlinear actuator provides an

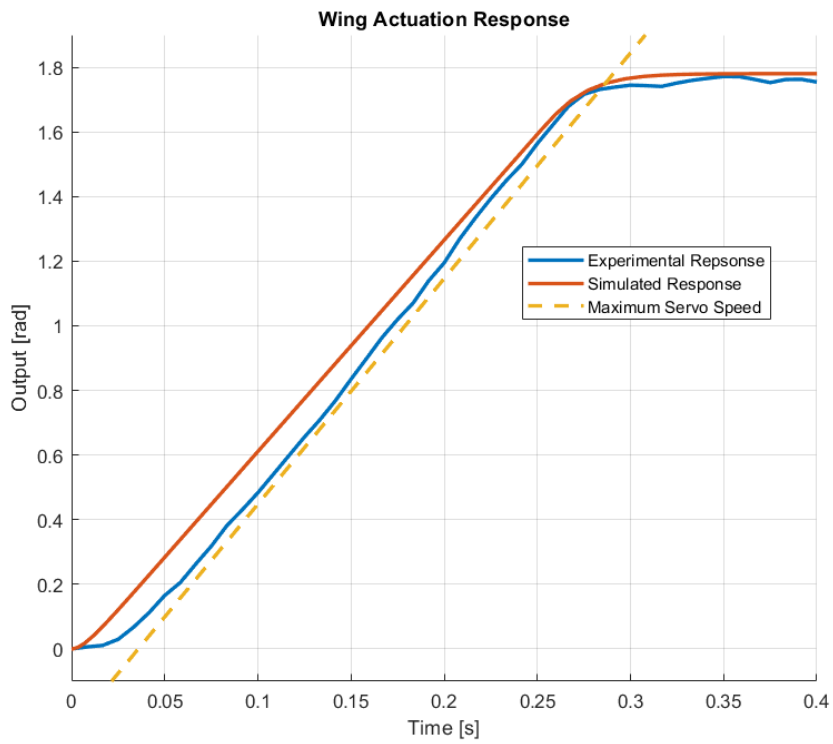


Figure 2.2: Experimental servo response (red) compared to the maximum servo speed (yellow) and an equivalent simulated servo (blue)

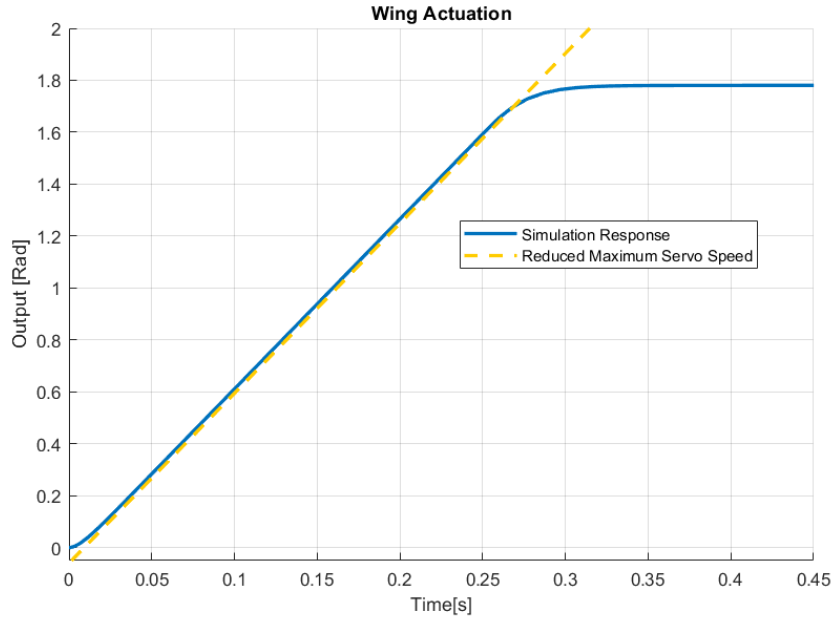


Figure 2.3: Simulated servo response (red) compared to the reduced maximum servo speed (yellow)

accurate estimation of the servos nonlinear response.

The motor response is modeled with a similar method using a second order system. The motor response was characterized by experimentally testing a test motor platform with a step input. A test motor, a 920KV 2212 BLDC motor, was installed on a test stand with the modeled power systems. The motor was given a step input from idle to full throttle while the prop rotation rate was recorded using and IR sensor. The data was put through a low pass filter to get a trend of the response to a desired rotation rate. Using the same method as the wing actuator response the motor rotation rate is modeled as a linear second order actuator with a maximum rate limit. The experimental data and the output of the equivalent simulated motor response are shown in figure 2.4.

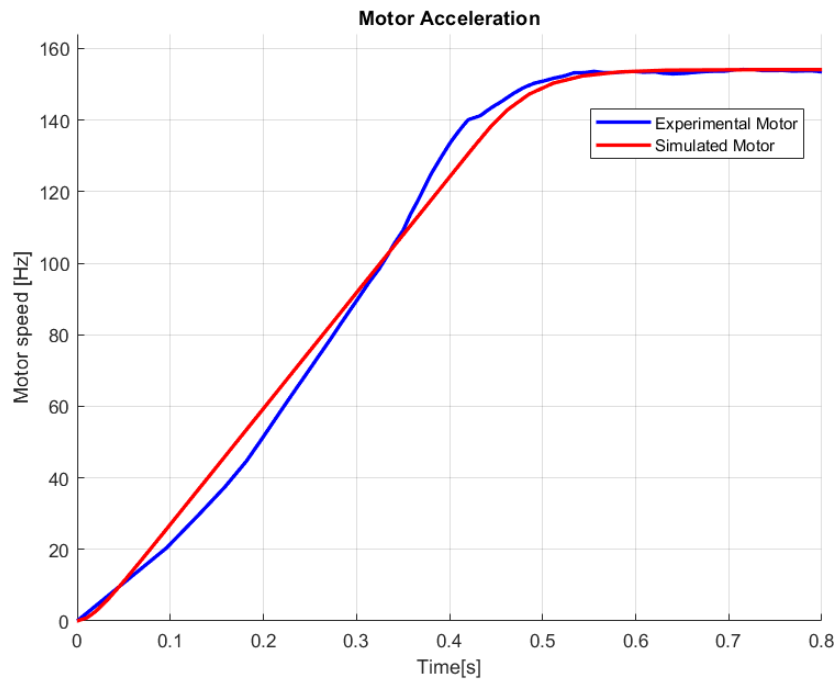


Figure 2.4: Experimental motor response (blue) compared to simulated motor response (red)

The motor rotation rate is calculated with a simplified model of systems components. With the given motor KV rating and system’s nominal battery voltage, the rotation rate was calculated in eq 2.5.

$$\omega_m = N_{cell}V_{cell}KV_{motor}(2\pi/60) \quad (2.5)$$

In order to accurately model the resulting force output from the motor, thrust data from the modeled APC 10.5x4.5 propeller is used. The output from this propeller was published in [40] which studied the output of propeller at tested rotation speeds and axial velocities. The results from the database are used in a lookup table to get the resulting propeller output. With the motor speed and axial velocity at the mounting point of each motor, the resulting motor thrust and drag moment can be accurately modeled. The motor speed is modeled as the throttle as a percent of the maximum rotation rate ω_m . These results are shown in figures 2.5 and 2.6 .

Each wing was modeled as continuous NACA0012 wings. These wings were selected based on the availability of data at high angles of attack. The final data used for the wing coefficient are published in [41]. During transition the wings will leave the conventional flight regime for an aircraft wing, so the model needs a wing that has been researched at high angles of attack. The wing aerodynamics effects were calculated from the local velocity of the defined actuator points. The angle of attack provided a lift, drag, and moment coefficient in 2.6. The airfoil coefficient data is shown in figure 2.7.

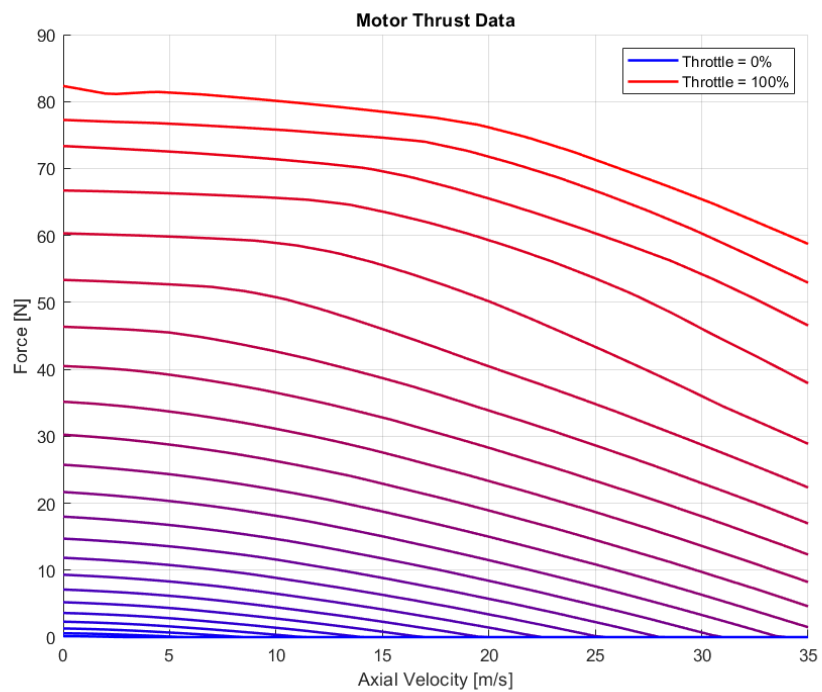


Figure 2.5: Thrust data for APC 10x4.5 propeller vs axial airspeed and throttle.

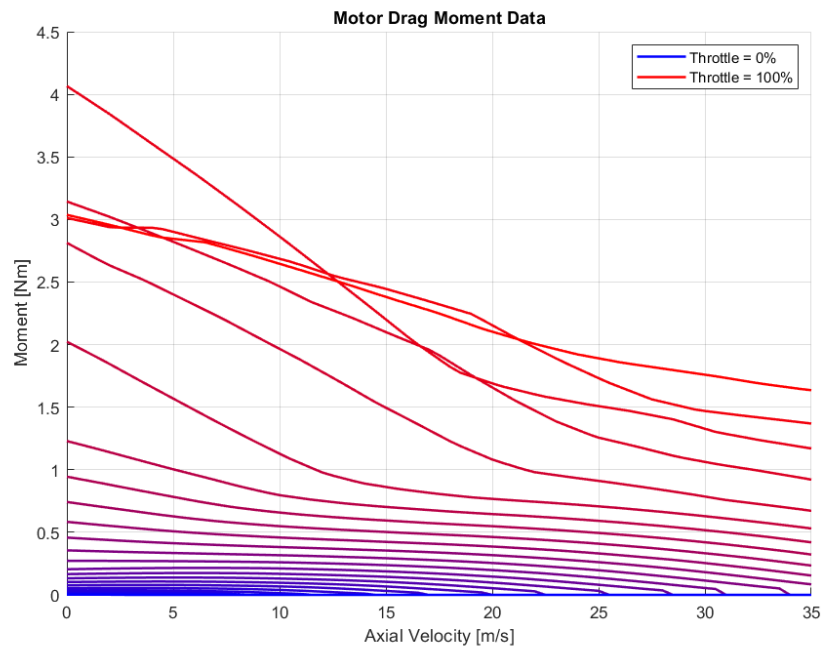


Figure 2.6: Drag moment data for APC 10x4.5 propeller vs axial airspeed and throttle.

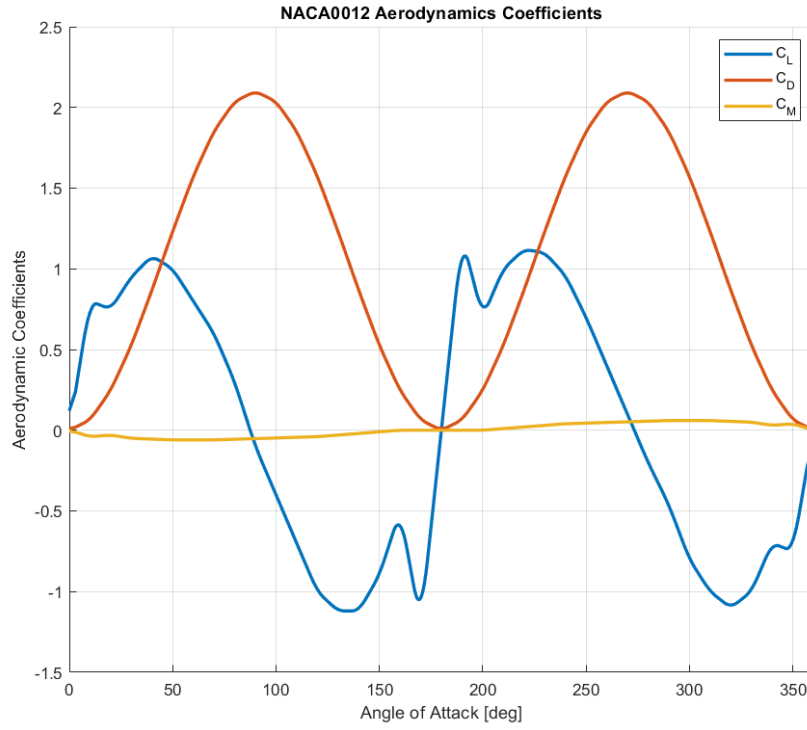


Figure 2.7: NACA0012 Airfoil Coefficients for any angle of attack.

$$Lift = C_l(\alpha)qA_{wing} \quad (2.6)$$

$$Drag = C_d(\alpha)qA_{wing} \quad (2.7)$$

$$Moment = C_m(\alpha)qA_{wing}c \quad (2.8)$$

In addition to the induced lift and drag from longitudinally moving air, the drag from the laterally moving air is added by modeling the area of the airfoil with a drag coefficient of 1. The area is calculated by integrating the edge definition of the NACA0012 airfoil.

The conservation of rotational energy is approximated to model the effect of actuating the wings through 2.9. The equivalent moment generated by actuating the wing is equal to the product of the inertia of the wing actuator about the rotation axis and the rotation speed, determined by the modeled non linear wing actuation.

$$M_y = I_{wing,y} \dot{\gamma} \quad (2.9)$$

Chapter 3: Control Strategy

3.1 Transition solver

In order to analyze and control the simplified test vehicle throughout the transition between hover and forward flight, the model's flight regimes need to be characterized. Throughout the transition the dynamics of the system change, therefore a method to characterize the dynamics based on the level of transition is necessary. Depending on the degree of nominal wing incident angle of the wing actuators γ , the level of transition the system reaches a steady state. The evolution of the steady states through the transition defines the transition corridor. Each point in the transition corridor defines the nominal wing actuator tilt, forward velocity, and motor speed. Similarly to the approach taken in [21], these parameters are used to create a linear model that can be stabilized through conventional linear controllers. To compute the steady state of the transition, the forces are balanced to find a steady state at each level of wing incident angle. This model assumes straight and level flight. The actuators are assumed to be in the same state, the same motor rotation rate and wing incident angle. All the moments generated by the actuators are balanced out to provide a net zero moment to the vehicle with exception of the wing moment coefficients which are neglected for this model. These assumptions are used

in a transition solver to compute the steady state at each point during transition. Each iteration of the solver computes the steady state of the vehicle defined by the angle nominal angle of the wing actuator, from fully upright 90° to fully forward to approximately 1.745° at a resolution of approximately 0.5° . This range completely models the flight regimes that the vehicle would encounter at a high enough resolution to accurately model the transition as a continuous set of dynamics. Each iteration starts by computing the set of all possible horizontal component of thrust, $T_{thrust,x}$, for the given transition angle. The set of forward velocity, v , for each thrust is computed from the set of the forward thrust components, such that the forward thrust is equal to the drag produced. The set of thrust produced results in an equivalent set of forward airspeeds. The airfoil data and the forward airspeed is used to generate the lift from the airfoils at each thrust level. The aerodynamics lift was combined with the vertical component of the thrust to get the total lift of the vehicle, F_z . To balance out the vertical components, one dimensional interpolation was performed on the total lift forces to find the thrust required, T_{req} , at which the lift equals the gravitational force on the vehicle.

$$F_{thrust,x} = T \cos(\gamma) \quad (3.1)$$

$$1/2\rho v^2(4C_{d,wing}bc + C_{d,body}A_{body,x}) = F_x \quad (3.2)$$

$$v = \sqrt{\frac{4F_x}{1/2 * \rho * (4C_{d,wing} + C_{d,body})}} \quad (3.3)$$

$$F_{lift,z} = 1/2\rho v^2 4C_l \quad (3.4)$$

$$F_z = F_{Lift,z} + T_{req} \sin(\gamma) \quad (3.5)$$

$$F_z = mass * g \quad (3.6)$$

$$v = \sqrt{\frac{T_{req} \cos(\gamma)}{1/2\rho(4C_{d,wing}bc + C_{d,body}A_{body,x})}} \quad (3.7)$$

With the horizontal airspeed and the required thrust the final throttle value is interpolated from the required thrust through the propeller data. The solver does not initially account for the decreased maximum thrust due to a non-zero axial velocity. Additionally, the propeller data does not model the loss of thrust past an axial velocity of 35m/s. These both result in an overestimation of the available thrust at higher transition levels and axial speeds. As a result, the solver does not reach an asymptote where the vehicle would need an unobtainable amount of thrust as would be expected at very high speed. This does not influence the data set because the vehicle does not transition to a point where the thrust can be overestimated. The resulting steady state for the model is shown in figures [3.1](#) and [3.2](#).

In addition to the steady state parameters of the transition corridor, the propeller data gives a measure of thrust efficiency which can be used to find the efficiency of flight at each point during transition. The efficiency η is described as a function of Thrust, axial velocity and power [\[40\]](#).

$$\eta = \frac{Thrust * V_{axial}}{P} \quad (3.8)$$

The propeller efficiency with the calculated forward velocity and propeller thrust the flight efficiency can be calculated.

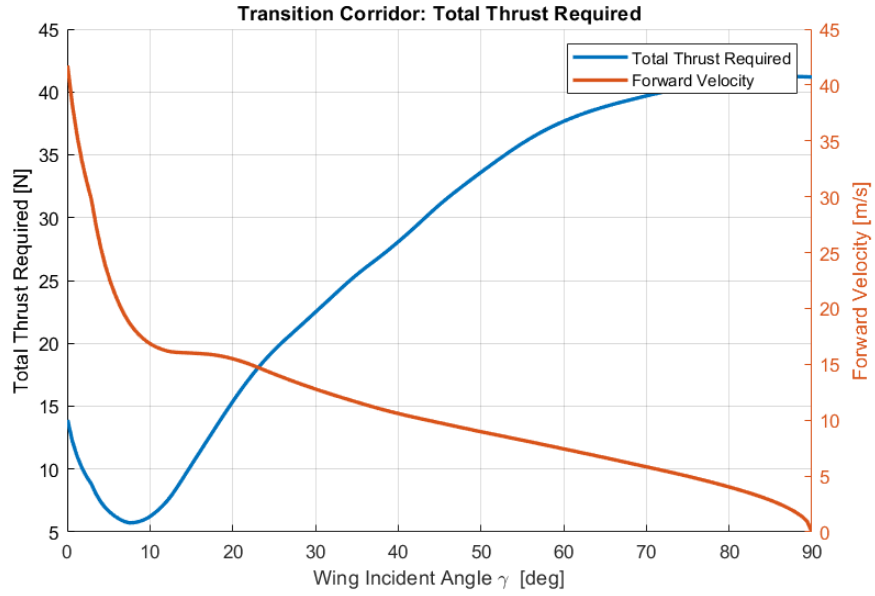


Figure 3.1: The total thrust required during transition plotted vs the steady state forward airspeed.



Figure 3.2: The throttle required during transition plotted vs the steady state forward airspeed.

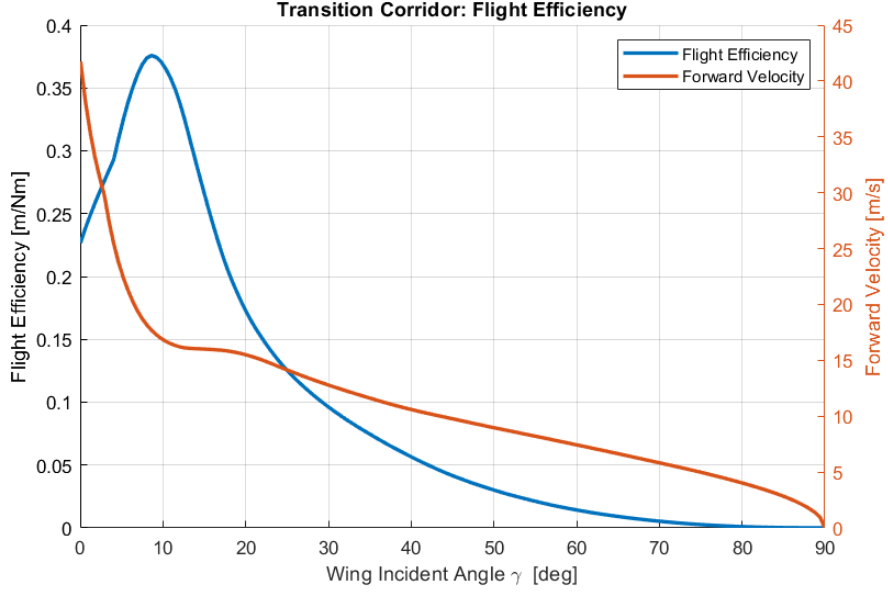


Figure 3.3: The flight efficiency during transition plotted vs the steady state forward airspeed. The maximum represents the most efficient flight envelope.

$$Efficiency = \frac{(\eta)}{T \cos(\gamma)} [m/J] \quad (3.9)$$

The flight efficiency through the transition corridor is shown in figure 3.3 and describes the point at which the transition is most efficient. This is the point where the increase in thrust required becomes more detrimental to efficiency than the benefits from increased lift from higher forward velocities. This point also defines the cruise point and the end of the transition corridor. The end of the transition accounts for the non-asymptotic transition calculations from the solver, as the vehicle will not transition to a point where the solver is inaccurate. The most efficient transition point is with wing incident angle, γ , of 8.64 degrees.

3.2 Controller Design

The vehicle's controller is designed to ensure that the vehicle maintains stability throughout the flight in any flight regime. The controller for the vehicle uses a LQR controller for stability in combination with PID outer loop controllers. All the controllers utilize gain scheduling to accurately control the vehicle at different positions throughout the transition corridor. The implementation of gain scheduling of the vehicle is defined by the vehicles wing incident angle. The nominal wing incident is used to define the steady state, which in turn defines the flight regime the controller assumes and functions according to. As a result of this the wing incident angle cannot rapidly change as the vehicle's assumed flight regime would diverge from the actual flight regime. The vehicle would not be able to accelerate or decelerate to the steady state and the controller would leave the designed flight regime, potentially resulting in an unstable controller. To ensure the vehicle does not deviate from the assumed flight regime, the magnitude of the change in nominal wing incident angle is constrained to a maximum value. During simulation this value is set as 10° per second. The intent of this research is based on the design of an eVTOL for passenger transport so slow transitions and smooth transition are a desirable result. The central part of the control method is the control of the vehicle's orientation. During transition the vehicles dynamics change such that the inputs to the system are highly nonlinear with respect to the scheduling parameter γ throughout the transition corridor. As a result the LQR stability controller encompasses the vehicles orientation while the outerloops can be handled through PID control

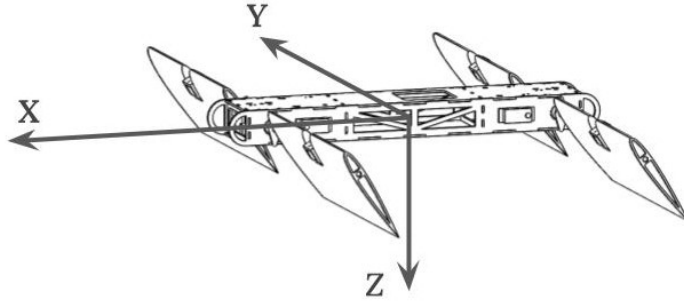


Figure 3.4: Definition of the vehicle body axis.

loops. Based on the vehicles calculated steady state, the system's orientation can be reduced to a linear state space model and a linear control policy can be developed. The model includes the vehicles Euler angles (ϕ, θ, ψ) and rotation rates $(\omega_\phi, \omega_\theta, \omega_\psi)$. The system is defined as shown in figure 3.4. The inputs to the system are the deviation of the vehicle's actuator from the steady state, defined as $[M_{1-4} \ W_{1-4}]$. The actuator conventions and input to the dynamics are defined as shown in fig 3.5. The system is linearized with respect to steady state given the wing incident angle, motor throttle, and forward velocity to build a linear parameter varying state space model defined in 3.10 - 3.11.

$$[A, B] = f(v_{ss}, \gamma_{ss}, throttle_{ss}) \quad (3.10)$$

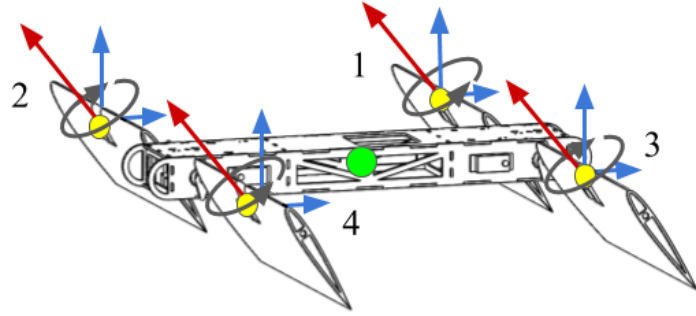


Figure 3.5: The conventions of the actuators and the input from each actuator. The contribution from the motor thrust (red), motor drag moment (grey), and aerodynamics lift/drag (blue) are modeled at the actuator point (yellow) about the center of mass (green).

$$A = \begin{bmatrix} \frac{d\dot{\phi}}{d\omega_\phi} & \frac{d\dot{\phi}}{d\phi} & \frac{d\dot{\phi}}{d\omega_\theta} & \frac{d\dot{\phi}}{d\theta} & \frac{d\dot{\phi}}{d\omega_\psi} & \frac{d\dot{\phi}}{d\psi} \\ 1 & 0 & 0 & 0 & 0 & 0 \\ \frac{d\dot{\theta}}{d\omega_\phi} & \frac{d\dot{\theta}}{d\phi} & \frac{d\dot{\theta}}{d\omega_\theta} & \frac{d\dot{\theta}}{d\theta} & \frac{d\dot{\theta}}{d\omega_\psi} & \frac{d\dot{\theta}}{d\psi} \\ 0 & 0 & 1 & 0 & 0 & 0 \\ \frac{d\dot{\psi}}{d\omega_\phi} & \frac{d\dot{\psi}}{d\phi} & \frac{d\dot{\psi}}{d\omega_\theta} & \frac{d\dot{\psi}}{d\theta} & \frac{d\dot{\psi}}{d\omega_\psi} & \frac{d\dot{\psi}}{d\psi} \\ 0 & 0 & 0 & 0 & 1 & 0 \end{bmatrix} \quad (3.11)$$

$$B = \begin{bmatrix} \frac{d\dot{\phi}}{dM_1} & \frac{d\dot{\phi}}{dM_2} & \frac{d\dot{\phi}}{dM_3} & \frac{d\dot{\phi}}{dM_4} & \frac{d\dot{\phi}}{dW_1} & \frac{d\dot{\phi}}{dW_2} & \frac{d\dot{\phi}}{dW_3} & \frac{d\dot{\phi}}{dW_4} \\ 0 & 0 & 0 & 0 & 0 & 0 & 0 & 0 \\ \frac{d\dot{\theta}}{dM_1} & \frac{d\dot{\theta}}{dM_2} & \frac{d\dot{\theta}}{dM_3} & \frac{d\dot{\theta}}{dM_4} & \frac{d\dot{\theta}}{dW_1} & \frac{d\dot{\theta}}{dW_2} & \frac{d\dot{\theta}}{dW_3} & \frac{d\dot{\theta}}{dW_4} \\ 0 & 0 & 0 & 0 & 0 & 0 & 0 & 0 \\ \frac{d\dot{\psi}}{dM_1} & \frac{d\dot{\psi}}{dM_2} & \frac{d\dot{\psi}}{dM_3} & \frac{d\dot{\psi}}{dM_4} & \frac{d\dot{\psi}}{dW_1} & \frac{d\dot{\psi}}{dW_2} & \frac{d\dot{\psi}}{dW_3} & \frac{d\dot{\psi}}{dW_4} \\ 0 & 0 & 0 & 0 & 0 & 0 & 0 & 0 \end{bmatrix} \quad (3.12)$$

With the linearized state space system model 3.13, the controller can return the optimal control strategy, 3.15, given the cost function defined in 3.14. The focus of the research is the creation of a robust control method through transition, therefore the state estimation is not modeled and the system is assumed to be completely observable. Using the solution from transition corridor, control strategy can be computed for discrete points in the transition corridor. These points are defined by the nominal wing incident angle. For the orientation controller, the feedback matrix K was defined from a wing incident angle of 90 degrees, hovering, to approximately 1.745 degrees, beyond optimal forward flight. These discrete points were calculated at intervals of 0.01 radians and the resulting feedback matrix K is linearly interpolated between to get a continuous feedback policy.

$$\dot{x} = Ax + Bu \quad (3.13)$$

$$J = \int (x^T Qx + u^T Ru) dt \quad (3.14)$$

$$u = -Kx \tag{3.15}$$

Initial values for the state and input weight matrices were set to the identity matrix and were tuned until a stable output was achieved. These weights were also varied as a function of the nominal wing incident angle. The final output for the input and state weighted matrices are shown in figure 3.6 with respect to the scheduling parameter γ . The evolution of the feedback matrix varying the scheduling parameter γ , is shown in figure 3.7. The linear feedback is able to stabilize the poles of the aircraft at all points throughout transition, figure 3.8.

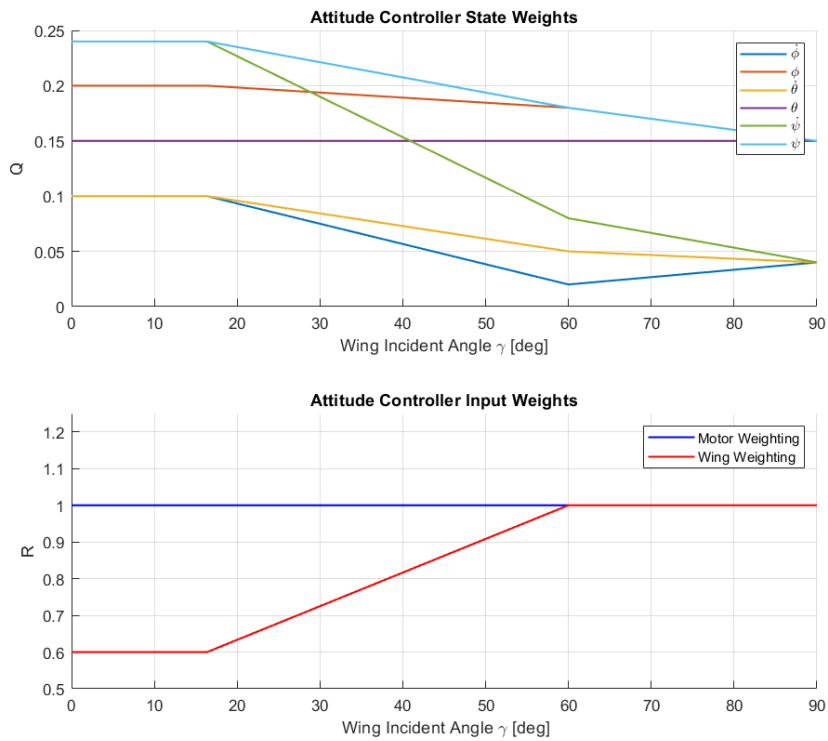


Figure 3.6: The scheduling of the LQR controller weights.

Beyond control of the orientation, the vehicle uses outerloop PID controllers

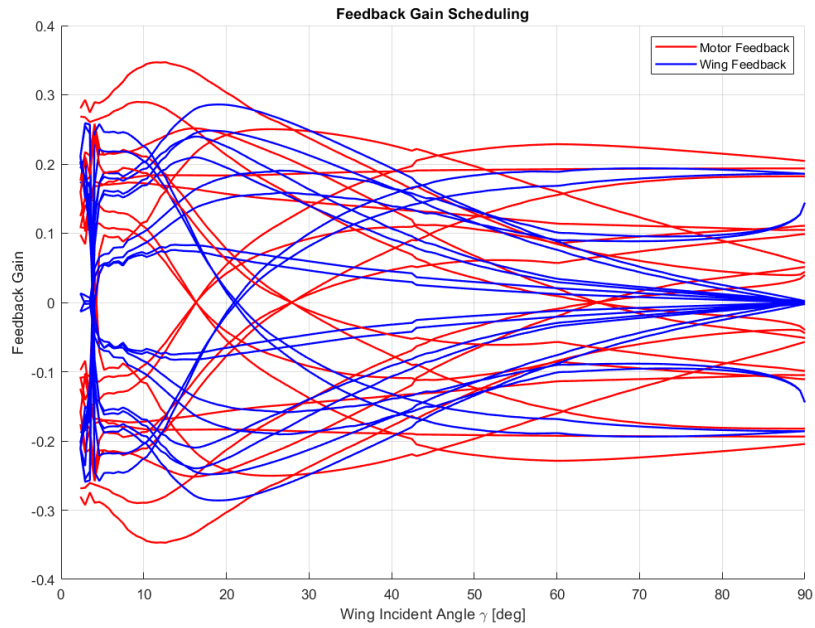


Figure 3.7: The evolution of the feedback gains throughout transition.

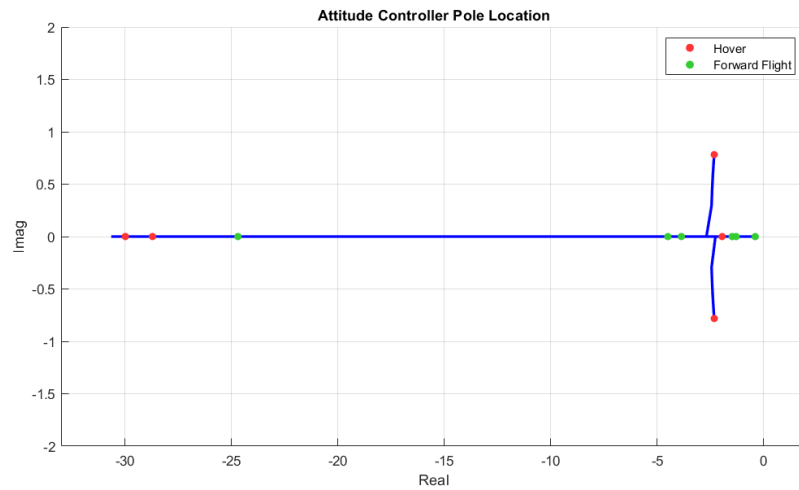


Figure 3.8: Attitude controller pole locations through transition.

to control the position and trajectory. The outerloop controllers contain an altitude controller and positional controller. Each PID was tuned through simulation until a

steady output was achieved. The altitude controller uses two gain scheduling PIDs to relate the error from desired altitude to throttle and desired pitch output. Initially in hover the altitude controller corrects for the altitude with changes in throttle similar to a conventional multi-copter. As the vehicle transitions into forward flight the controller is varied to correct the altitude by changing the vehicles pitch like a conventional fixed-wing aircraft. The positional controller is separated into two flight regimes, hovering and forward flight. The controllers are interchanged based on whether the vehicle is in hover or if the nominal wing incident angle is vertical. The hover controller uses the conventional control policies of a multi-copter where the desired velocity is controlled through a calculated roll and pitch attitude. The calculated desired attitude is rotated by the vehicles current yaw so it is able to correct its position separately from the desired vehicle heading. The controller feeds the desired roll and pitch attitudes along with the desired vehicle heading as yaw into the LQR attitude controller to achieve the desired attitude. When the vehicle is in forward flight, the desired position is achieved through coordinated turns to achieve the desired heading. The controller assumes the vehicle is some degree of forward flight and corrects the error in desired heading towards the target position through a coordinated roll and yaw inputs. These outputs are again fed into the LQR attitude controller to achieve the desired attitude. The outer loop control strategy is shown in figure 3.9.

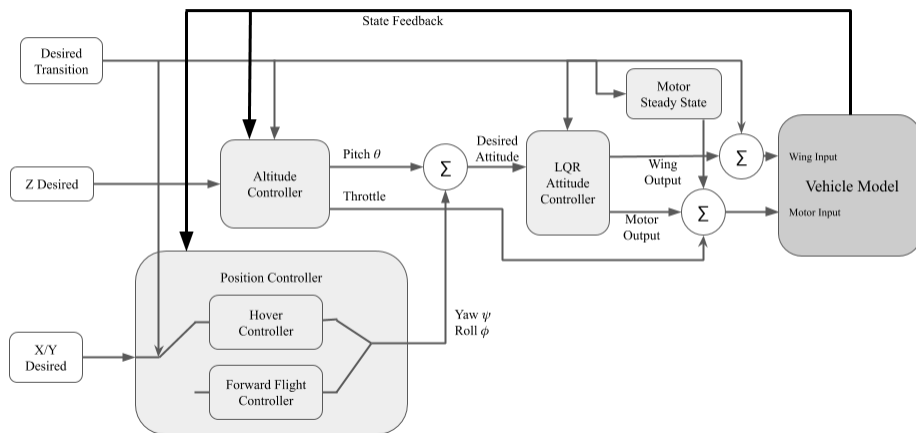


Figure 3.9: Overview of the Controller Systems

Chapter 4: Simulations

4.1 3DOF Simulation

In order to test the robustness of the proposed eVTOL transition controller, the nonlinear model of the simplified test vehicle was built in MATLAB/SIMULINK. This simulation was used as a platform to develop the control policies and test the robustness of the controller. To test control throughout transition, the first simulation was setup to model the longitudinal dynamics of the vehicle. This model initially simplified the model to a three degree of freedom (3DOF) simulation to incorporate the dynamics of the transition while excluding the lateral stability. This allowed for development and testing of the vehicles transition control strategy before moving to the full 6 degrees of freedom (6DOF) simulation. For this simulation the LQR attitude controller was reduced to the pitch variables, θ and ω_θ .

The 3DOF simulation was simulated using the 3DOF body fixed simulation in MATLAB/SIMULINK. The body was simulated as the vehicle's center of mass and uses the model's mass and longitudinal inertia properties. The input to the system are the forces on the XZ plane F_z and F_x on the body's center of mass and the moment generated around it M_y . The inputs were calculated from the model and actuator states.

For the longitudinal simulation the output of the actuators were assumed to be laterally symmetric since the simulation does not model the lateral dynamics. In this simulation the motor moments were ignored as the lateral symmetry would cancel the resulting effects.

In order to test the robustness of the controller design the model was subjected to input disturbances. The model was disturbed to test the vehicles ability to maintain stability and stay within a regime where the linear LQR attitude controller can correct errors. These disturbances were modeled from random zero mean white Gaussian noises at 0.25 second intervals. The disturbances were added to the input moment and forces up to a standard deviation of approximately 2.75 Nm and 10.3 N respectively. The maximum standard deviation magnitude of the input moment and forces were modeled from the equivalent moment and forces of one of the motors at steady state hover. This is a higher disturbance then the vehicle would experience during normal operation and represents a worst case scenario.

To verify the calculations of the transition corridor the experimental data during a transition can be compared to the result of the calculated transition corridor. The transition was simulated by transitioning the wing incident angle from fully vertical to horizontal over 50 seconds and recording the forward speed. The input disturbances are neglected for this simulation to get the true steady state of the vehicle. This comparison is shown in figure [4.1](#). The results for this simulation are conservative compared to the steady state at each transition point as the simulation is continuously transitioning over the simulated time and needs time to accelerate to the actual steady state. This is represented in the graph as the simulated velocity is

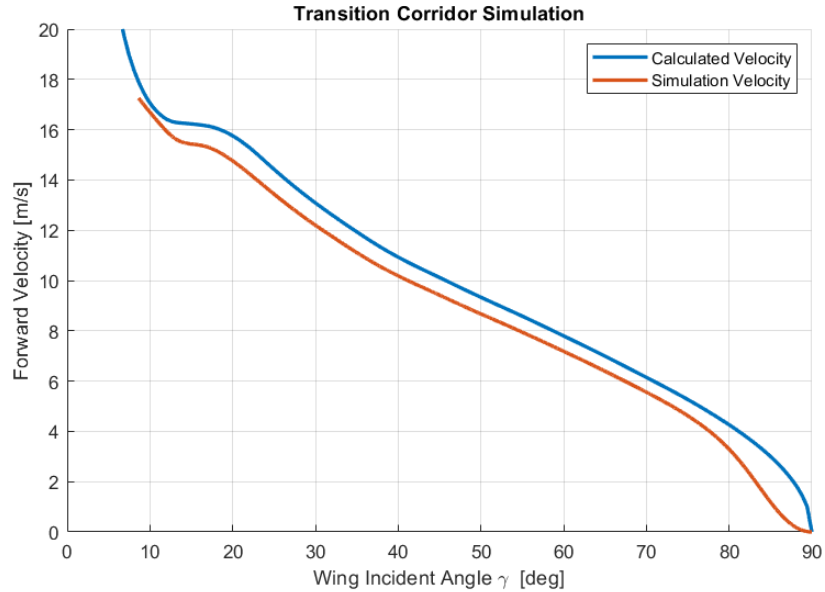


Figure 4.1: Comparison of calculated transition corridor and a simulated transition corridor.

slightly lower than the calculated velocity. This is especially prevalent at transition angles close to vertical. These angles would require significantly more time to reach steady state as the forward acceleration is very small relative to the drag a low speed and again this discrepancy is shown in the results. The simulated calculated transition corridor agrees with the simulation and can therefore be used to design the gain scheduling of the attitude controller.

To verify that the controller can robustly keep the vehicle stable during transition, the vehicle was initially simulated from hover into forward flight. The input disturbances were set to the maximum magnitude. The wing incident angles during the transition is shown in figure 4.2. The incident angle of the wings started vertically during hover, and transitioned to the full forward flight angle over approx-

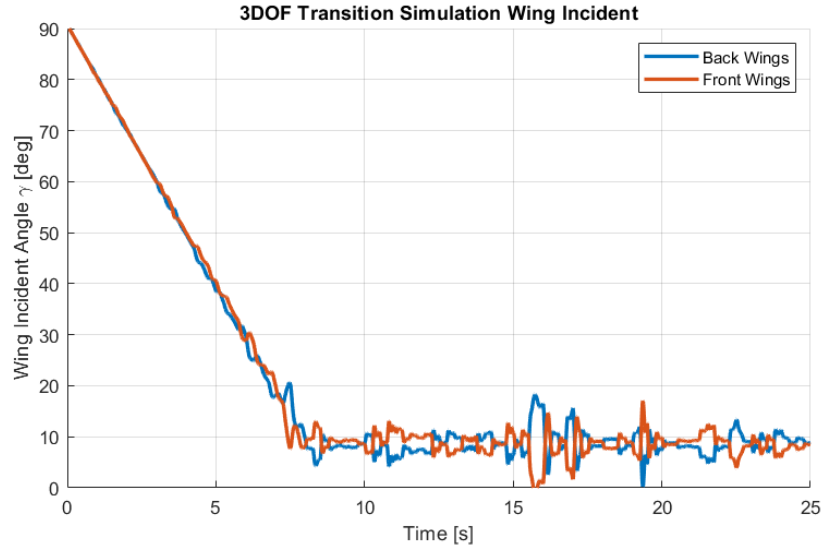


Figure 4.2: Wing incident angle of the front and back wings from a 3DOF simulation of the vehicle transitioning from hover to forward flight.

imately 8 seconds. As the vehicle transitioned into forward flight the wings become the dominant method to correct for attitude disturbances and deflect from the nominal value with greater magnitude. Conversely the motors provide the entirety of the ability to correct the attitude while the vehicle is near hover so in figure 4.3, the motor output from the motors pairs, initially the output is very noisy as it the only method to correct the attitude. As the vehicle transitions into forward flight, the responsibility of correcting the attitude moves from the motors to the wing actuators, so the output of the motors settle. The motors deviate less for correction and follow longer oscillatory trends as a result of correcting for altitude.

The attitude of the vehicle during the transition are shown in figure 4.4. If the vehicle attitude deviates to far from the steady state attitude the actuators will become saturated and the vehicle will not be able to return to the steady state

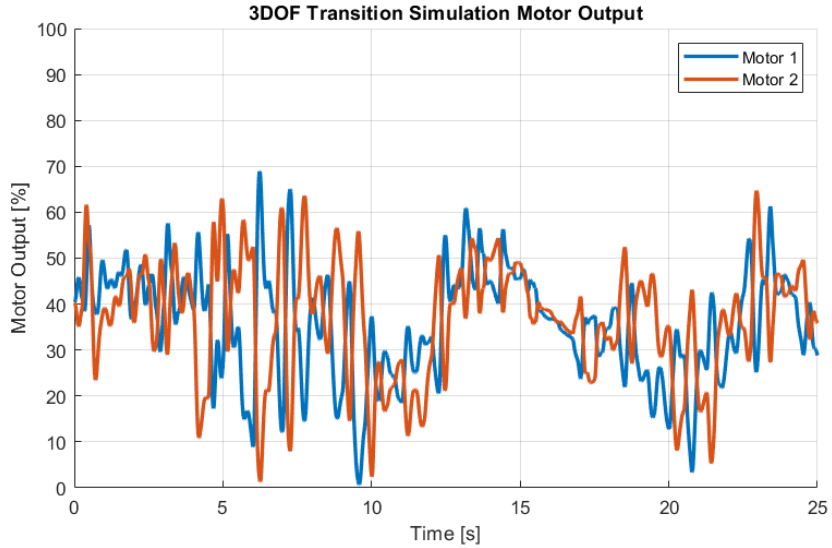


Figure 4.3: Motor output, as a percent of the possible rotation speed, of the front and back wings from a 3DOF simulation of the vehicle transitioning from hover to forward flight.

attitude. The large input disturbances cause large deviations in the vehicle output however the vehicle remains stable and controllable throughout transition. The input disturbances and attitude deviations also cause a deviations in the global velocity, shown in figure 4.5, but again do not destabilize the vehicle.

To test the full functionality of the controller and its ability to work as a vehicle for transport, the model was tasked with completing a simulated full transport mission. The vehicle would have to take off to a certain altitude, transition to forward flight, return to hover, and land at the desired location. During this simulation the vehicle was tasked with ascending to an altitude of 10 meters and traveling 500 meters before landing again. Because the goal is to test the ability of the vehicle to execute a designed mission and not purely maintain stability, the input disturbances

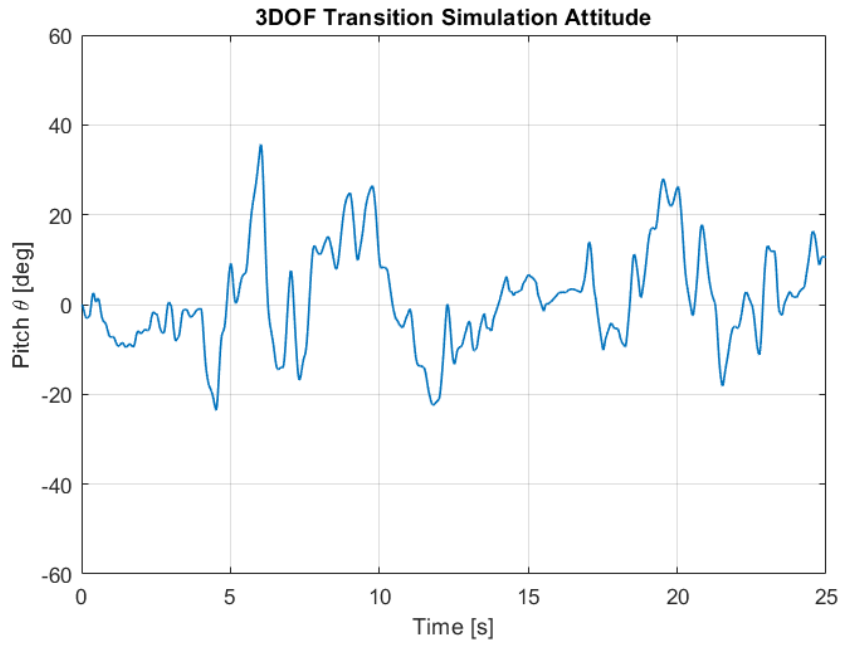


Figure 4.4: Vehicle Attitude from a 3DOF simulation of the vehicle transitioning from hover to forward flight.

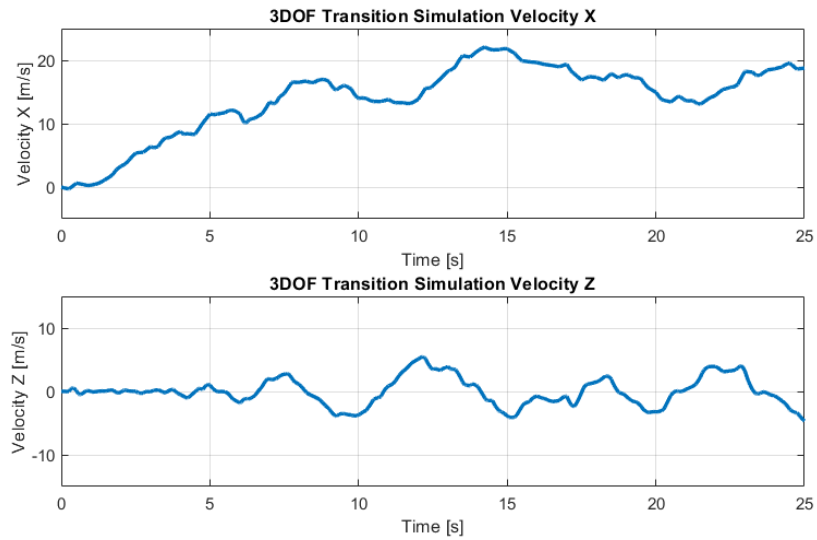


Figure 4.5: Vehicle global velocity from a 3DOF simulation of the vehicle transitioning from hover to forward flight.

are model a 25 percent of the maximum normal input. The actuator output data from the simulations are shown in figures 4.6 and 4.7. The wing incident angles transitioned to the forward flight where it stayed there for approximately 20 seconds before transitioning back to hover. From figure 4.9, during the forward flight phase of the mission the vehicle reached a steady forward flight velocity of approximately 18 m/s which agrees with the calculated steady state from the transition corridor. The vehicle reaches the desired goal of 500 meters and maintains relatively close desired altitude of 10 meters during the simulation from figure 4.8. At approximately 40 seconds the vehicle reaches hover and the hover controller takes over position control. In figure 4.10, a sustained pitch is held to slow the vehicle and move to the desired final position with the hover controller. To model the transition the vehicle's state can be plotted in the transition corridor vs the calculated steady state in figure 4.11. As the vehicle transitions to forward flight and back to hover the assumed nominal steady state wing incident angle, γ_n , deviates from the true angle because the airspeed needs time to reach the steady state, however it does not deviate enough to destabilize the vehicle.

4.2 6DOF Simulation

With the transition simulated through the longitudinal simulation, the model can be extended to the full 6 degrees of freedom to model the full vehicle dynamics. The model is extended to include the full position and attitude states, X , Y , Z , ϕ , θ , and ψ .

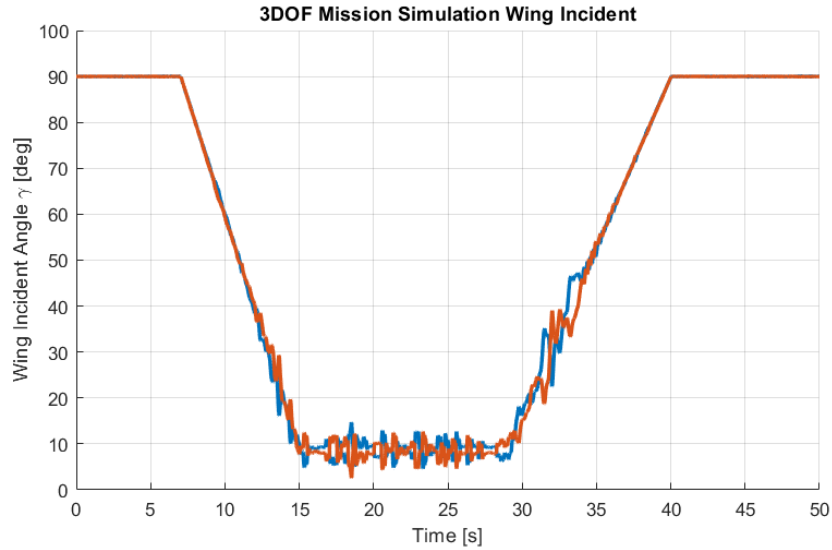


Figure 4.6: Wing incident angles of the front and back wings for a simulated mission.

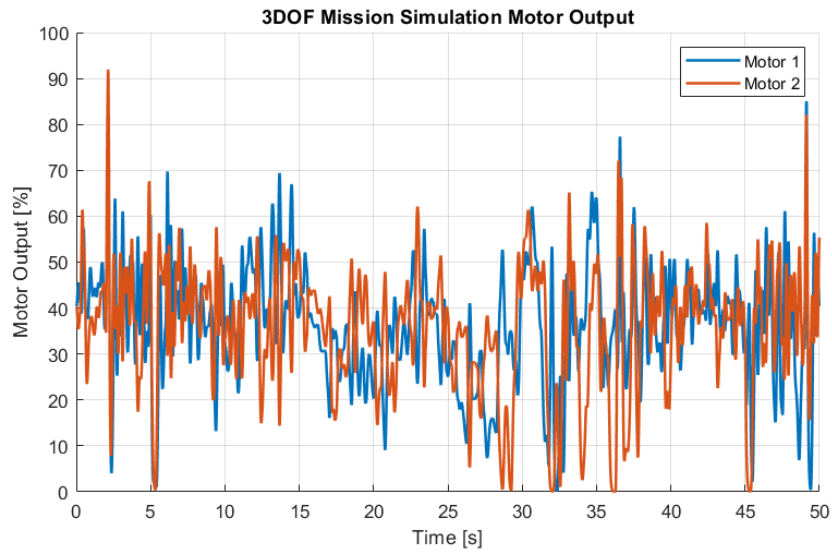


Figure 4.7: Motor output, as a percent of the possible rotation speed, of the front and back motors for a 3DOF simulated mission.

With independent control of each actuator the rotational moments and propeller drag moments are no longer assumed to cancel out due to lateral symmetry.

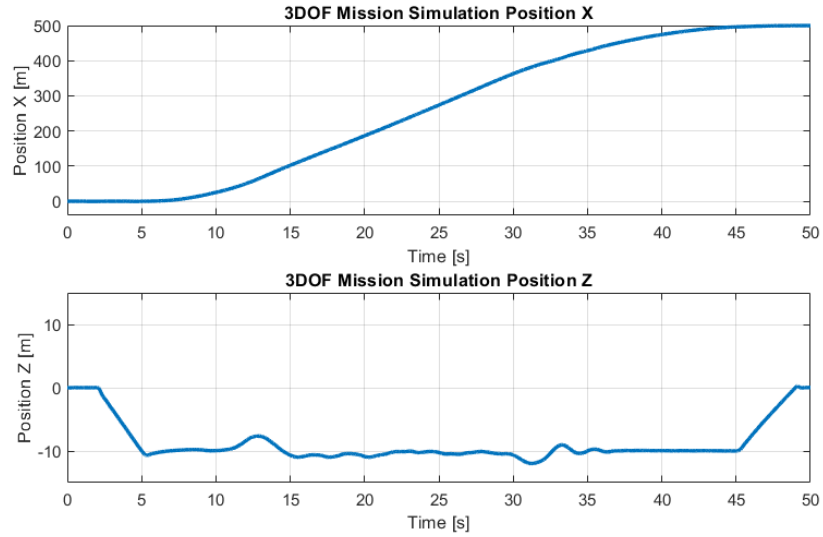


Figure 4.8: Vehicle position for a 3DOF simulated mission. Vehicle rises to 10 meters before traveling 500 meters where it lands at 0 meters.

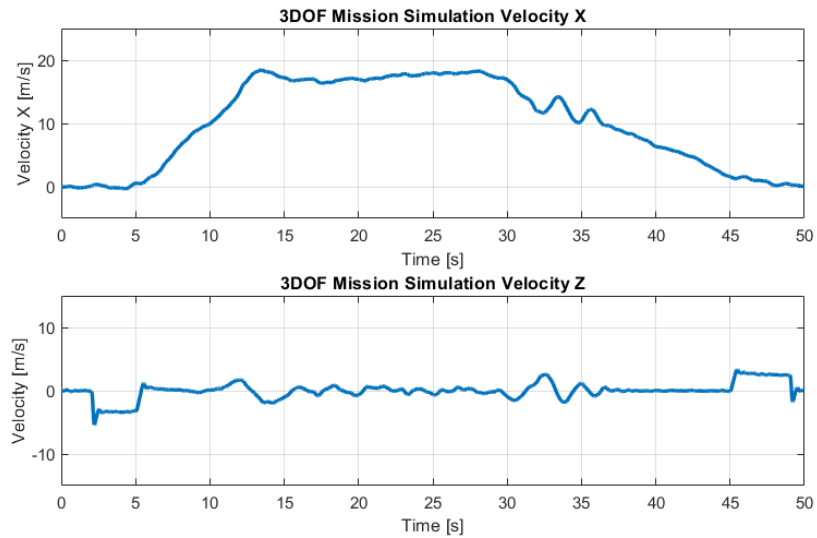


Figure 4.9: Vehicle global velocity for a simulated mission.

The moment from each propeller is added along the axis of the of the motor in the opposite direction of the rotation of the propeller. The applied moment is defined

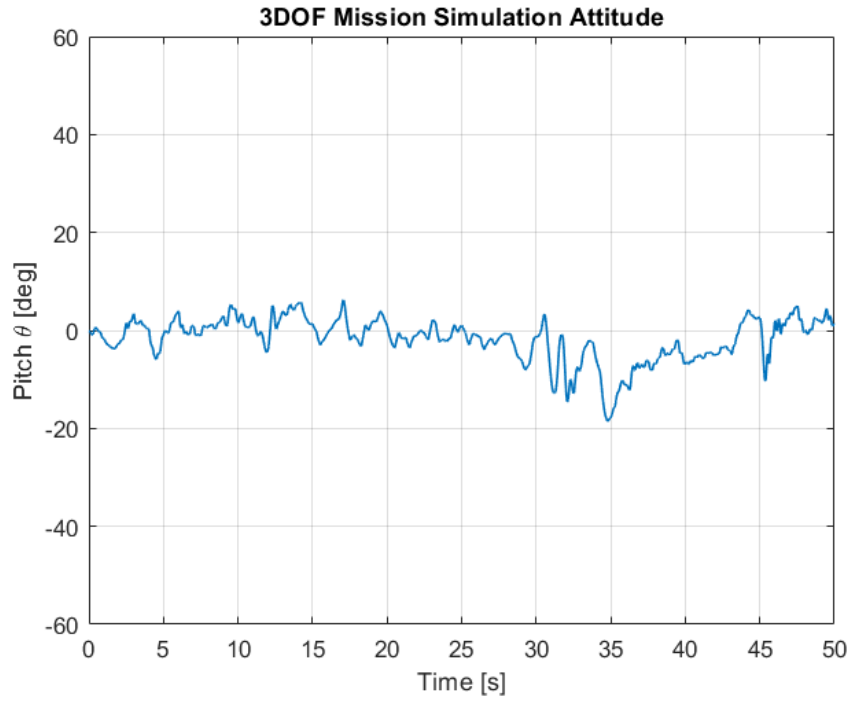


Figure 4.10: Vehicle attitude during a 3DOF simulated mission.

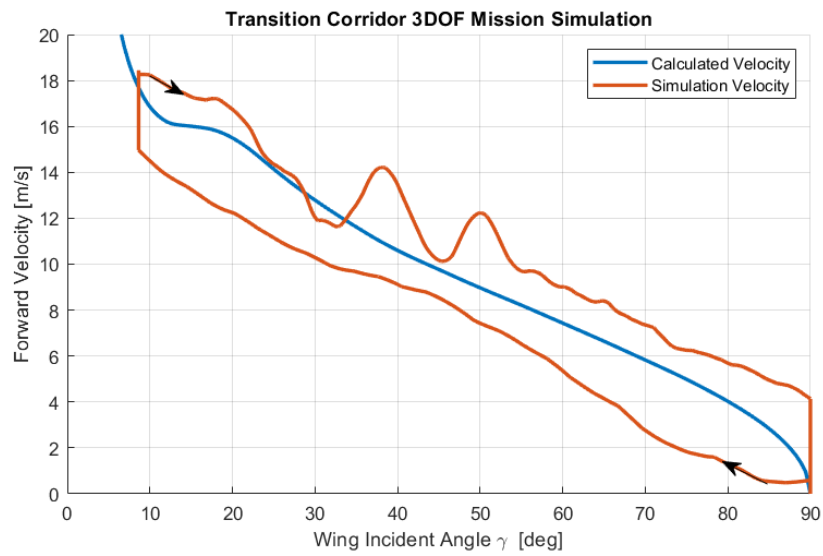


Figure 4.11: Vehicle's path through the transition corridor during the simulated mission

in figure 3.5. The input disturbances are expanded to the additional dimensions. The maximum input disturbance force is kept the same at the force of one motor at hover but is applied to every axis. The maximum input disturbance torque is calculated as the applied torque from the motor at hover. The torque input for each axis is based on the configuration of the vehicle as it is multiplied by the distance to the axis of rotation. The disturbance torque applied to the Z axis of the vehicle is calculated as equivalent to the X axis disturbance because the motor applies force in the XZ plane with distance l_x . To test the robustness of the controller throughout the transition corridor in with six degrees of freedom the model was again simulated through a transition simulation and a simulated mission profile. The transition simulation tested the controllers ability to transition from hover to forward flight. The input disturbances were again set to the maximum in an attempt to destabilize the vehicle. The results from the simulation are shown in figures 4.12 - 4.16.

Throughout the transition and into forward flight the vehicle remained stable. The controller was able to correct for the external disturbances and reach a steady state in full forward flight. Compared to the 3DOF simulation results, the 6DOF had significantly higher deviations. This is expected as the attitude controller has two additional axis to stabilize and the nonlinear effects of deviations between multiple axis are not modeled well within the linearized model. This is in figure 4.16 seen around 19 seconds into the simulation where all the attitude states simultaneously have large deviations. Even though the input disturbances cause very large deviations, it remains within a controllable range. In forward flight the steady state velocity reaches a higher forward velocity of approximately 22 m/s. This is due

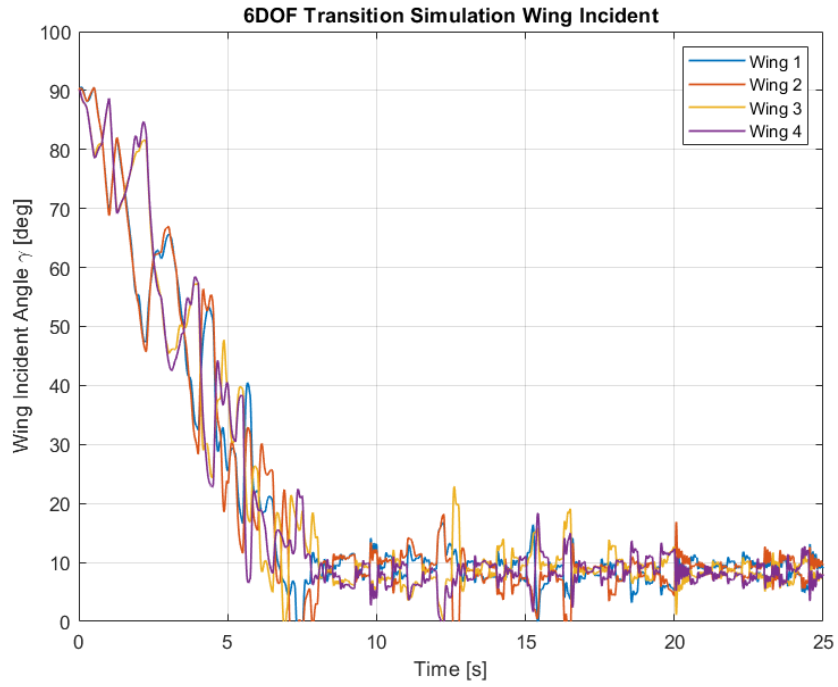


Figure 4.12: Wing incident angles for a simulated transition in 6DOF.

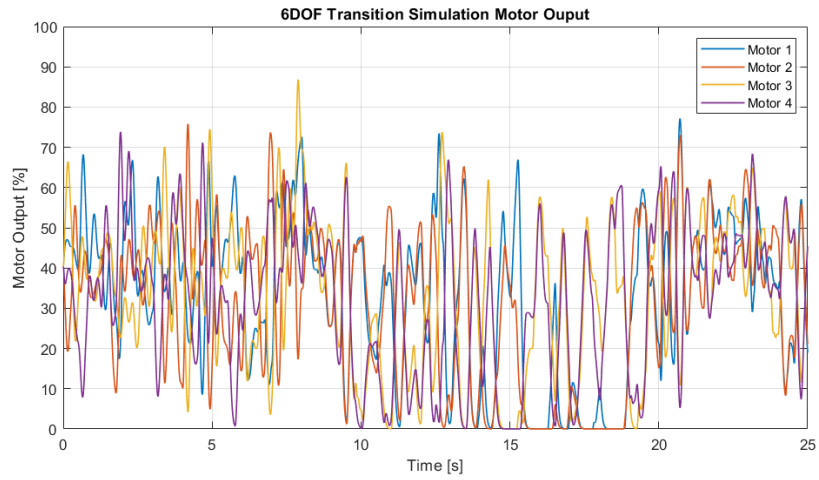


Figure 4.13: Motor output, as a percent of the possible rotation speed, for a 6DOF simulated transition.

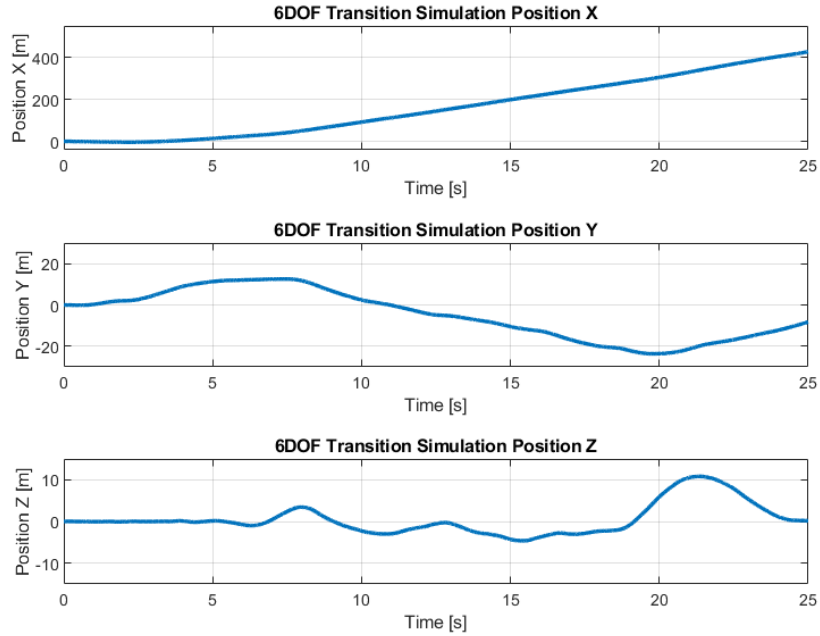


Figure 4.14: Vehicle position for a 6DOF simulated transition from hover to forward flight.

to the linearization of the motor input. The input from the motors is modeled as linear with regards to the motor rotation speed. This relationship is more closely represented through the equation in 4.1. As the controller linearly decreases and increases the left and right pairs separately to correct the vehicle's yaw, the total forward thrust does not remain constant. The total forward thrust is greater then in the steady state which leads to a higher forward velocity. This can be fixed by rearranging the input matrix to the attitude LQR controller as the force from the motor and back out the required throttle.

$$T = k_f \omega_m^2 \tag{4.1}$$

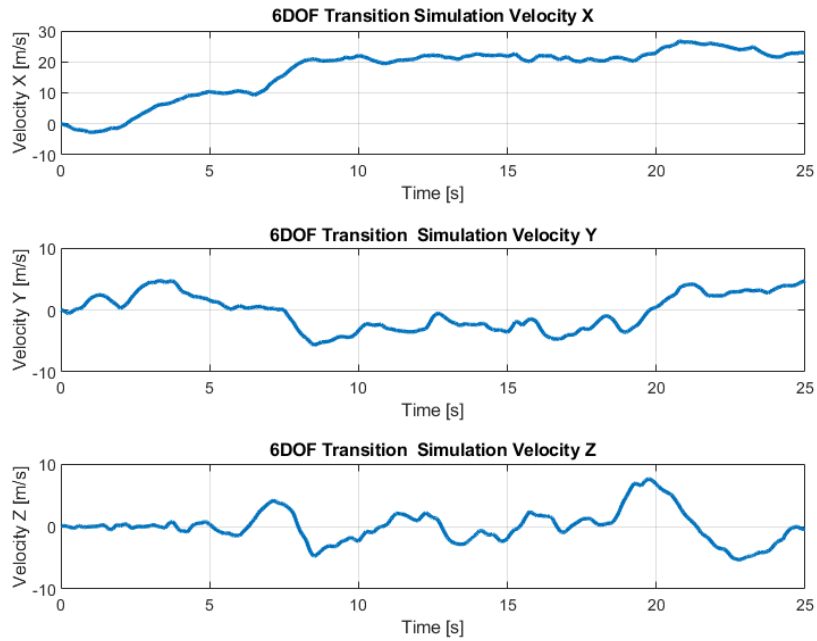


Figure 4.15: Vehicle global velocity for a 6DOF simulated transition from hover to forward flight.

The vehicle is again tested with the transport mission profile as defined for the 3DOF mission simulation. The vehicle takes off to 10 meters where it transitions into forward flight. It continues to the destination at 500 meters forward, where it transition backs to hover and lands. The results for this simulation are shown in figures 4.17 - 4.22.

Figure 4.19 shows the position of the vehicle throughout the simulated mission. Over the course of the simulation time the vehicle converges on the desired position of 500 meters. During the mission the input disturbances cause the vehicle to deviate in the Y direction, but the heading controller brings vehicle back to the desired trajectory. The global velocity, shown in figure 4.20, indicates the

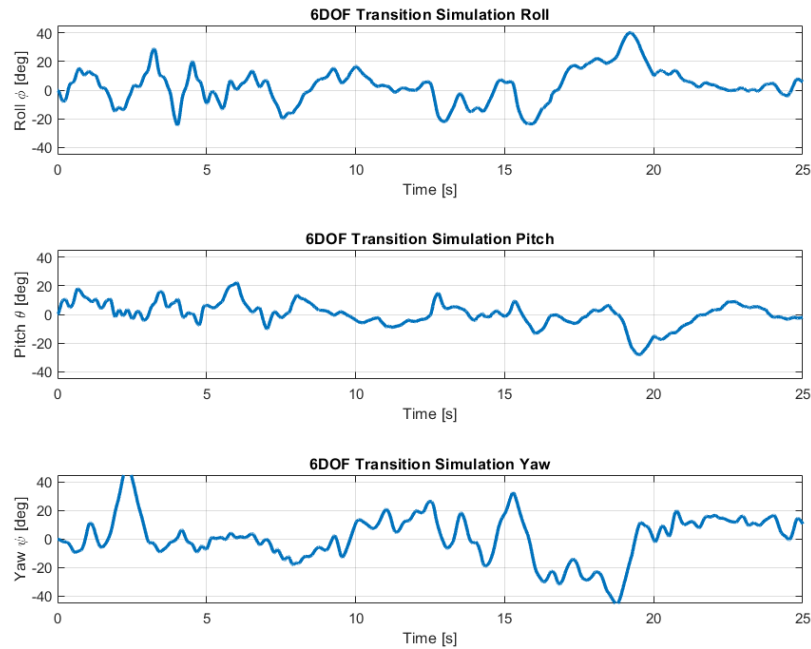


Figure 4.16: Vehicle attitude during a 6DOF simulated transition from hover to forward flight.

vehicle transitioning into forward flight and reaching a steady forward flight velocity of approximately 19 m/s before returning to hover. The velocity has noticeable deviations in the X and Z velocity around 32 and 36 seconds into the flight which are supported by deviations in the pitch attitude in figure 4.21. The deviations are caused by the assumed flight regime deviating from the actual flight regime during transitioning back to hover, however are not significant enough to destabilize the vehicle. This is also seen in figure 4.22 when the transition presents large deviations from the calculated transition when return to hover or a wing incident angle of 90° .

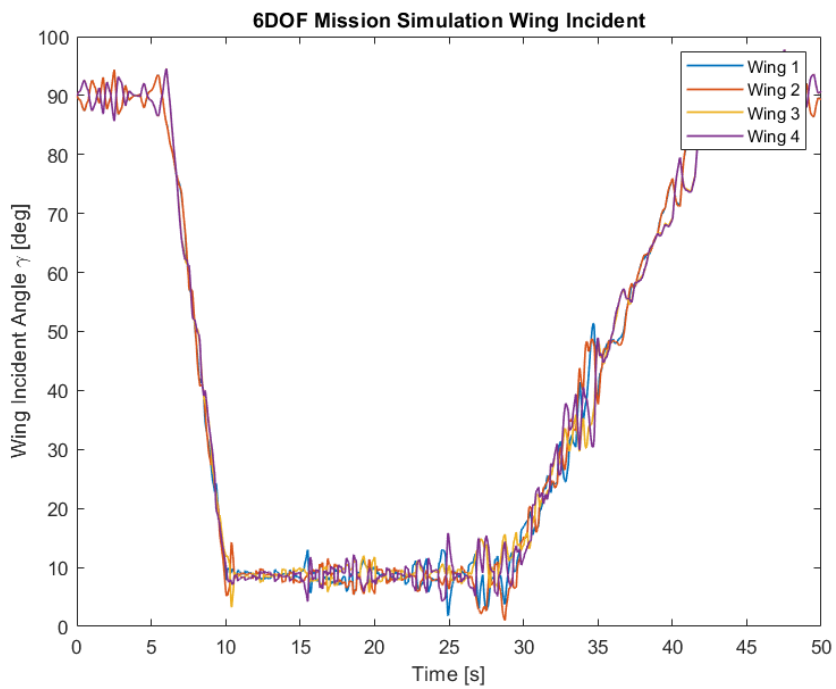


Figure 4.17: Wing incident angles for a simulated mission profile in 6DOF

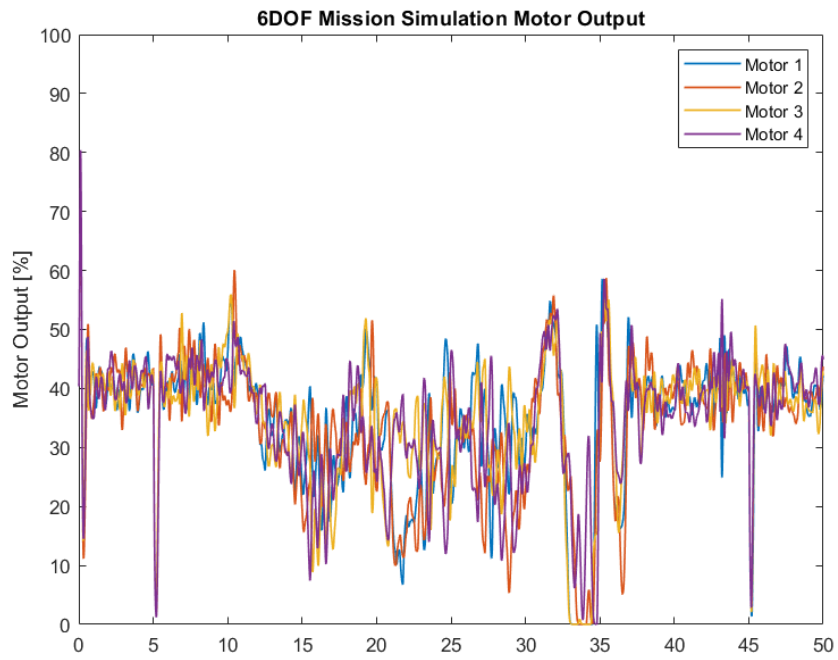


Figure 4.18: Motor output, as a percent of the possible rotation speed, for a simulated mission profile in 6DOF.

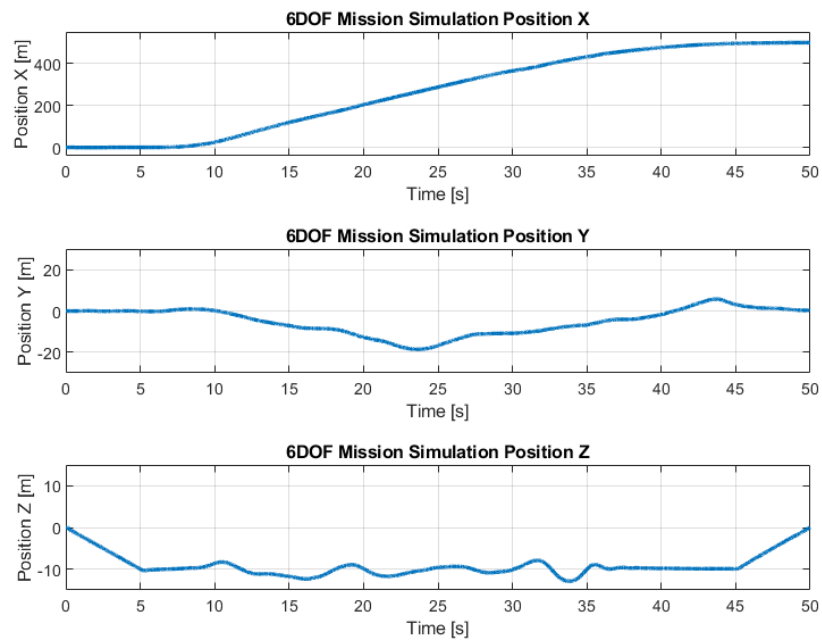


Figure 4.19: Vehicle position for a simulated mission profile in 6DOF

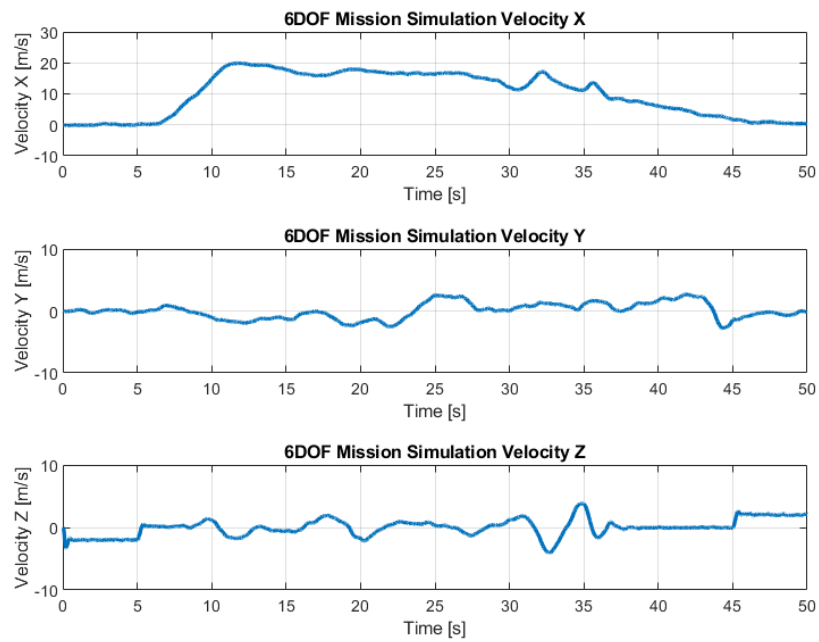


Figure 4.20: Vehicle global velocity for a simulated mission profile in 6DOF

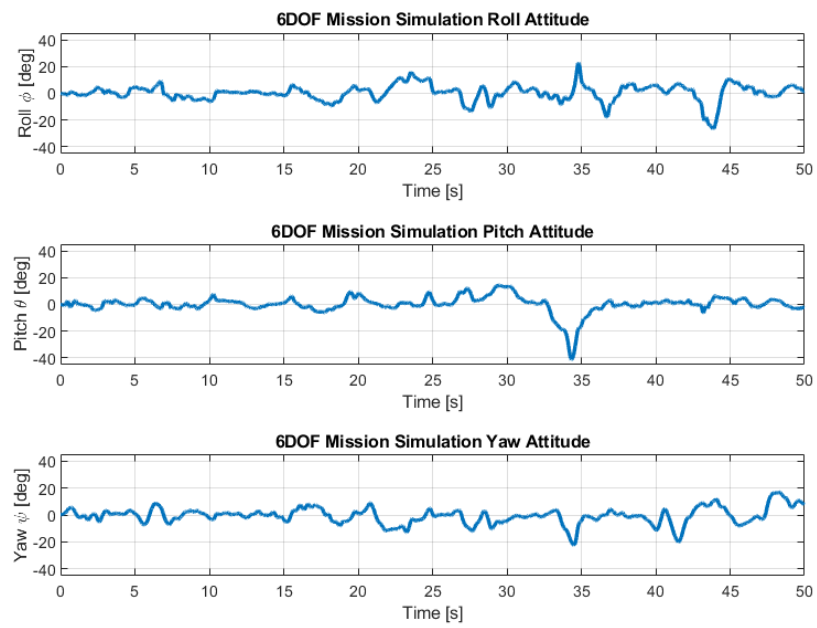


Figure 4.21: Vehicle attitude for a simulated mission profile in 6DOF

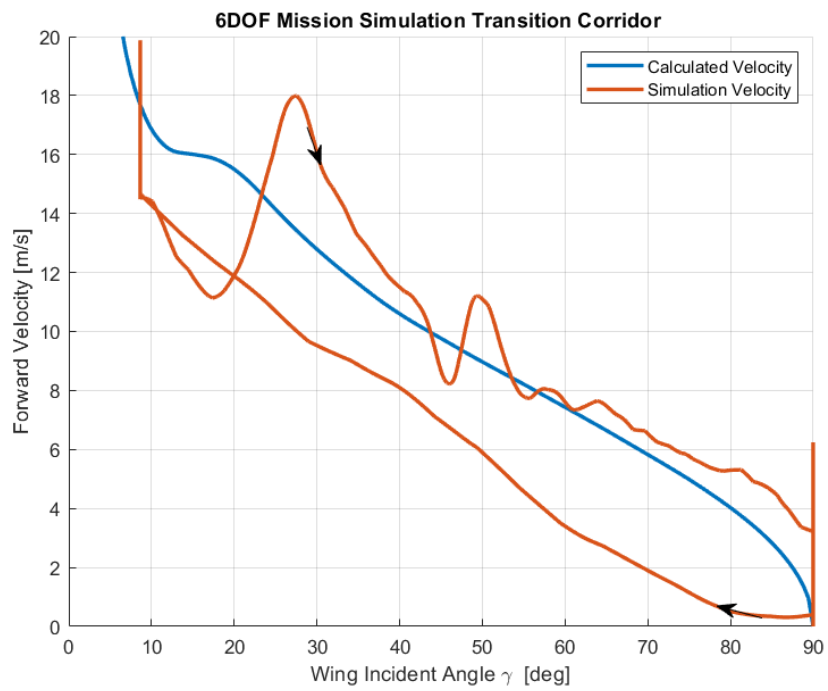


Figure 4.22: Vehicle transition corridor path for a simulated mission profile in 6DOF

Chapter 5: Conclusion

5.1 Summary of Contributions

The goal of this research was to produce an effective strategy to control an eVTOL vehicle throughout all phases of transition. By establishing a vehicle model and effectively characterizing the dynamics at discrete points throughout the transition, the transition corridor for this model was developed. This allowed for characterization of the model steady state and development of the steady state linearization. Using the linearized model and the parameters from the actuator model, an optimal feedback policy was implemented to control the vehicle attitude. The attitude controller was combined with outerloop PID controllers to fully control the vehicle's trajectory. The controllers implemented gain scheduling to control the vehicles dynamics as they change throughout the transition. To verify the control strategy's robustness, a nonlinear model of the vehicle was constructed in a 3DOF and 6DOF simulation. In each of the tests the proposed strategy was able to maintain the vehicles stability in the presence of large disturbances. The vehicle was stable throughout transition and was able to complete the mission profiles. The proposed strategy provides a robust method to control an eVTOL vehicle throughout transition.

5.2 Future Work

While this research offered an effective method to control an eVTOL through transition, there are still improvements and further exploration that should be completed. This method provided is not a final solution to the problem, but rather an investigation and assessment of the methodology of transition control. The transition corridor was defined by the transition angle and the flight regimes associated at that steady state. This can be an optimistic assumption because input disturbances or quick changes to the nominal incident angle can cause the vehicle to diverge from the assumed steady state and make the vehicle become less stable. Further research in defining the transition corridor as a two-dimensional function of forward velocity and nominal wing incident angle would help resolve this problem. It is not feasible for the vehicle to operate solely at steady state so expanding the controller to adjust to flight regimes that deviate from the calculated steady state will give the vehicle more flexibility in transition and overall improve the controllers robustness. Another limitation of this research is that it focuses on the implementation of the vehicle's controller. The application of a controller to a vehicle is a combination of estimation and control. This research assumes that the states are fully observable and does not account for the potential errors in estimation. The implemented LQR controller would realistically be apart of a larger Linear Quadratic Gaussian (LQG) solution where the state would be optimally estimated. Finally, the results of the controller's robustness from the simulation are subject to the level of fidelity the simulation can achieve. The tests are simulated version of the true model dynamics

and therefore are only an estimate of the effectiveness of the control strategy. The model provides a good approximation of the dynamics, however there are numerous ways in which the simulation can be improved. The outputs of the wings were approximated through lookup tables with simplified models. This does not model the more complex aerodynamics effects of the wings or more importantly the interactions and effects between subsets of actuators. The actuators act decoupled and therefore do not model interactions like the effects of multiple airfoils in a flow stream or the change in aerodynamics coefficients due to the forced airflow from the motor over the wing. Each part of the model is an approximation of the dynamics and can be improved. Taking this point to the furthest extent, the ideal product of this research would be implementing the proposed control strategy on a real-world test platform. This entails creating a platform that can represent the described eVTOL model, calculating the dynamics and control policies through the process detailed in this research, and testing the robustness of the control strategy through experimental trails.

Bibliography

- [1] Mark Williamson. Air power the rise of electric aircraft. *Engineering Technology*, 9(10):77–79, November 2014. Conference Name: Engineering Technology.
- [2] Vishwanath Bulusu and Raja Sengupta. Urban Air Mobility: Viability of Hub-Door and Door-Door Movement by Air. March 2020.
- [3] N Goel and J Holden. Uber Elevate: Fast-Forwarding to a Future of On-Demand Urban Air Transportation, April 2017.
- [4] William Pickell, Andrew Kopeikin, Elizabeth Bristow, and James Bluman. Feasibility Study for a MEDEVAC Electric UAS Capability. In *2019 International Conference on Unmanned Aircraft Systems (ICUAS)*, pages 630–635, June 2019. ISSN: 2373-6720.
- [5] J. J. Alonso, Heather M. Arneson, John Melton, Michael Vegh, Cedric F. Walker, and Larry A. Young. System-of-Systems Considerations in the Notional Development of a Metropolitan Aerial Transportation System. [Implications as to the Identification of Enabling Technologies and Reference Designs for Extreme Short Haul VTOL Vehicles With Electric Propulsion]. 2017.
- [6] CityAirbus. URL: <https://www.airbus.com/innovation/urban-air-mobility/vehicle-demonstrators/cityairbus.html>.
- [7] Uber Elevate | Uber Air. URL: <https://www.uber.com/us/en/elevate/uberair/>.
- [8] PAV – eVTOL Passenger Air Vehicle – Aurora Flight Sciences. URL: <https://www.aurora.aero/pav-evtol-passenger-air-vehicle/>.
- [9] D F Finger, C Braun, C Bil, and Bundoora Vic. The Impact of Electric Propulsion on the Performance of VTOL UAVs. *CEAS Aeronautical Journal*, 10:827–843, 2019.
- [10] Venturiold. URL: <http://hopflyt.com/venturiold/>.

- [11] Adnan S. Saeed, Ahmad Bani Younes, Shafiqul Islam, Jorge Dias, Lakmal Seneviratne, and Guowei Cai. A review on the platform design, dynamic modeling and control of hybrid UAVs. In *2015 International Conference on Unmanned Aircraft Systems (ICUAS)*, pages 806–815, June 2015. ISSN: null.
- [12] Joby Aviation. URL: <https://www.jobyaviation.com/>.
- [13] Heaviside. URL: <https://kittyhawk.aero/heaviside/>.
- [14] Introducing the Liliu Jet - Liliu. URL: <https://liliu.com/the-jet>.
- [15] ASX | Airspace Experience Technologies | Detroit MI | VTOL. URL: <https://www.iflyasx.com>.
- [16] D. J. Leith and W. E. Leithead. Survey of gain-scheduling analysis and design. *International Journal of Control*, 73(11):1001–1025, January 2000. Publisher: Taylor & Francis .eprint: <https://doi.org/10.1080/002071700411304>.
- [17] Pedro Casau, David Cabecinhas, and Carlos Silvestre. Hybrid Control Strategy for the Autonomous Transition Flight of a Fixed-Wing Aircraft. *IEEE Transactions on Control Systems Technology*, 21(6):2194–2211, November 2013. Conference Name: IEEE Transactions on Control Systems Technology.
- [18] David Vorsin and Shai Arogeti. Flight transition control of a multipurpose UAV. In *2017 13th IEEE International Conference on Control Automation (ICCA)*, pages 507–512, July 2017. ISSN: 1948-3457.
- [19] Tianxing Chang, Zhiming Guo, Jiawei Zhang, and Liaoni Wu. Landing Control Scheme of Vertical Takeoff and Landing Fixed-wing UAV. In *2018 IEEE 3rd Advanced Information Technology, Electronic and Automation Control Conference (IAEAC)*, pages 1984–1988, October 2018. ISSN: 2381-0947.
- [20] Vincenzo Muscarello and Giuseppe Quaranta. Simulation of Tiltrotor Manuevers Using Linear Parameter Varying Models. ERF 2017, 2017. Curran Associates.
- [21] Zilun Zhang, Tielin Ma, Shuai Hao, Zhuoqi Wang, and Yi Liu. Design of A Distributed Propulsion VTOL UAV. In *2019 IEEE International Conference on Unmanned Systems (ICUS)*, pages 84–89, October 2019.
- [22] Hafiz Noor Nabi, Coen De Visser, Marilena Pavel, and Giuseppe Quaranta. A quasi-Linear Parameter Varying (qLPV) Approach for Tiltrotor Conversion Modeling and Control Synthesis. May 2019.
- [23] Chih-Chen Yih. Flight control of a tilt-rotor quadcopter via sliding mode. In *2016 International Automatic Control Conference (CACCS)*, pages 65–70, November 2016.

- [24] Hou Shunxiang and Ling Rui. Tracking control for underactuated VTOL aircraft. In *2017 29th Chinese Control And Decision Conference (CCDC)*, pages 1646–1650, May 2017. ISSN: 1948-9447.
- [25] Jin H. Kim, S. Andrew Gadsden, and Stephen A. Wilkerson. Adaptive integral sliding mode controller for longitudinal rotation control of a tilt-rotor aircraft. In *2016 24th Mediterranean Conference on Control and Automation (MED)*, pages 820–825, June 2016.
- [26] Gong Haisheng and Liu Jinkun. Sliding Mode Control for VTOL Aircraft Based on High-Gain Observer. In *2012 Second International Conference on Instrumentation, Measurement, Computer, Communication and Control*, pages 305–309, December 2012. ISSN: null.
- [27] Zamri Omar, Cees Bil, and Robin Hill. The Application of Fuzzy Logic on Transition Manoeuvre Control of a New Ducted-Fan VTOL UAV Configuration. In *Second International Conference on Innovative Computing, Information and Control (ICICIC 2007)*, pages 434–434, September 2007.
- [28] Dongkyoung Chwa. Fuzzy Adaptive Output Feedback Tracking Control of VTOL Aircraft With Uncertain Input Coupling and Input-Dependent Disturbances. *IEEE Transactions on Fuzzy Systems*, 23(5):1505–1518, October 2015. Conference Name: IEEE Transactions on Fuzzy Systems.
- [29] Xiaoxing Fang, Qing Lin, Yingxun Wang, and Lili Zheng. Control strategy design for the transitional mode of tiltrotor UAV. In *IEEE 10th International Conference on Industrial Informatics*, pages 248–253, July 2012. ISSN: 2378-363X.
- [30] Inseok Yang, Dongik Lee, and Dong Seog Han. Designing a Robust Non-linear Dynamic Inversion Controller for Spacecraft Formation Flying. *Mathematical Problems in Engineering*, 2014. ISSN: 1024-123X Library Catalog: www.hindawi.com Pages: e471352 Publisher: Hindawi Volume: 2014.
- [31] Navya Thirumaleshwar Hegde, V. I. George, and C Gurudas Nayak. Modelling and Transition flight control of Vertical Take-Off and Landing unmanned Tri-Tilting Rotor Aerial Vehicle. In *2019 3rd International conference on Electronics, Communication and Aerospace Technology (ICECA)*, pages 590–594, June 2019.
- [32] E Cetinsoy, S Dikyar, C Hancer, K. T. Oner, E Sirimoglu, M. Unel, and M. F. Aksit. Design and construction of a novel quad tilt-wing UAV. *Mechatronics*, 22(6):723–745, September 2012.
- [33] B. Theys, G. De Vos, and J. De Schutter. A control approach for transitioning VTOL UAVs with continuously varying transition angle and controlled by differential thrust. In *2016 International Conference on Unmanned Aircraft Systems (ICUAS)*, pages 118–125, June 2016.

- [34] Vibhu Kumar Tripathi, Laxmidher Behera, and Nishchal Verma. Design of sliding mode and backstepping controllers for a quadcopter. In *2015 39th National Systems Conference (NSC)*, pages 1–6, December 2015.
- [35] Kaan Taha Öner, Ertugrul Cetinsoy, Mustafa Ünel, Mahmut Faruk Akşit, İlyas Kandemir, and Kayhan Gülez. Dynamic model and control of a new quadrotor unmanned aerial vehicle with tilt-wing mechanism. volume 35, pages 58–63, Paris, France, November 2008. WASET (World Academy of Science, Engineering and Technology).
- [36] Balázs Kulcsár. LQG/LTR CONTROLLER DESIGN FOR AN AIRCRAFT MODEL. *Periodica Polytechnica Transportation Engineering*, 28(1-2):131–142, 2000.
- [37] Yin Hang, Zhu Jihong, Yuan Xiaming, and Zhang Chao. Robust hover control of thrust-vectorred unmanned tail-sitter aircraft against gust load. In *2013 10th IEEE International Conference on Control and Automation (ICCA)*, pages 735–738, June 2013. ISSN: 1948-3457.
- [38] D777MG Servo. URL: <https://www.servocity.com/d777mg-servo>.
- [39] HS-55 Servo. URL: <https://www.servocity.com/hitec-hs-55-servo>.
- [40] J.B. Brandt, R.W. Deters, G.K. Ananda, and M.S. Selig. (Jan 10, 2020), UIUC Propeller Database, University of Illinois at Urbana-Champaign, retrieved from <http://m-selig.ae.illinois.edu/props/propdb.html>, March 2020.
- [41] Chris Critzos, Harry Heyson, and Robert Boswinkle. AERODYNAMIC CHARACTERISTICS OF NACA 0012 AIRFOIL SECTION. Technical report, NATIONAL ADVISORY COMMITTEE FOR AERONAUTICS, January 1955.